**Molecular Therapy**
Original Article

# Precise editing of FGFR3-TACC3 fusion genes with CRISPR-Cas13a in glioblastoma

Ye Wu,[1,2,7] Weili Jin,[1,2,7] Qixue Wang,[1,2] Junhu Zhou,[1,2] Yunfei Wang,[1,2] Yanli Tan,[3,4] Xiaoteng Cui,[1,2] Fei Tong,[1,2] Eryan Yang,[1,2] Jian Wang,[5,6] and Chunsheng Kang[1,2]

[1]Department of Neurosurgery, Tianjin Medical University General Hospital, Tianjin 300052, China; [2]Tianjin Neurological Institute, Key Laboratory of Post-neurotrauma Neuro-repair and Regeneration in Central Nervous System, Ministry of Education, Tianjin City, Tianjin 300052, China; [3]Department of Pathology, Hebei University School of Basic Medical Sciences, Hebei 071000, China; [4]Department of Pathology, Affiliated Hospital of Hebei University, Baoding, Hebei 071000, China; [5]Department of Neurosurgery, Qilu Hospital and Institute of Brain and Brain-Inspired Science, Shandong University, 107 Wenhua Xi Road, Jinan 250012, China; [6]Department of Biomedicine, University of Bergen, Jonas Lies Vei 91, 5009 Bergen, Norway

**FGFR3-TACC3 (F3-T3) gene fusions are regarded as a "low-hanging fruit" paradigm for precision therapy in human glioblastoma (GBM). Small molecules designed to target the kinase in FGFR currently serve as one form of potential treatment but cause off-target effects and toxicity. Here, CRISPR-Cas13a, which is known to directly suppress gene expression at the transcriptional level and induce a collateral effect in eukaryotes, was leveraged as a possible precision therapy in cancer cells harboring F3-T3 fusion genes. A library consisting of crRNAs targeting the junction site of F3-T3 was designed, and an *in silico* simulation scheme was created to select the optimal crRNA candidates. An optimal crRNA, crRNA1, showed efficiency and specificity in inducing the collateral effect in only U87 cells expressing F3-T3 (U87-F3-T3). Expression profiles obtained with microarray analysis were consistent with induction of the collateral effect by the CRISPR-Cas13a system. Tumor cell proliferation and colony formation were decreased in U87-F3-T3 cells expressing the Cas13a-based tool, and tumor growth was suppressed in an orthotopic tumor model in mice. These findings demonstrate that the CRISPR-Cas13a system induces the collateral damage effect in cancer cells and provides a viable strategy for precision tumor therapy based on the customized design of a CRISPR-Cas13a-based tool against F3-T3 fusion genes.**

## INTRODUCTION

The CRISPR-Cas system has been cleverly harnessed to carry out various genomic engineering tasks.[1] CRISPR-Cas13a (also known as C2c2) is a class 2, type VI CRISPR-Cas system.[2] Sequence analysis revealed that Cas13a lacked a recognized DNase catalytic site but comprised two highly conserved HEPN domains.[3] Therefore, Cas13a is capable of efficiently cleaving complementary target RNA, which acts as a single-RNA guided RNA-targeting CRISPR effector.[1] To date, the CRISPR-Cas13a system is thought to be an approach that directly suppresses gene expression at the transcriptional level. In comparison with Cas9, Cas13a contributes a potentially safer alternative because it results in loss-of-function phenotypes without losing targeted genes in the genome.[4] Recent studies have reported the crystal structure of *Leptotrichia shahii* (Lsh) Cas13a bound to crRNA and the apo form as well as the overall structure of the *Leptotrichia buccalis* (Lbu) Cas13a-crRNA-target RNA complex. These results provide considerable insight into the structurally detailed molecular mechanism of the function of Cas13a and set the stage for its future development as an RNA-targeting technology.[5,6] We anticipate a new era in personalized cancer therapy in which CRISPR-Cas13a serves as a vital link between bench and bedside.[7]

The FGFR3-TACC3 (F3-T3) fusion protein, first reported in glioblastoma (GBM) samples, has emerged as an oncogenic driver in a variety of cancers, including urothelial cancer, non-small cell lung cancer, cervical cancer, head and neck cancer, gastrointestinal malignancies, and malignant melanoma.[8–10] Approximately 1.2%–8.3% of GBMs have been predicted to harbor this translocation.[10] The genes coding for FGFR3 and TACC3, which reside on human chromosome 4p16, 48 kb apart, represent the most frequent rearrangement of FGFR-TACC in malignant glioma. FGFR-TACC fusions are potent oncogenes which have growth-promoting effects and induce aneuploidy. However, the intracellular signaling pathway is unclear.[11]

Tumors harboring FGFR-TACC fusions generally have a dismal clinical outcome.[12,13] Currently, no effective personalized therapy exists for the treatment of GBM. Thus, this fusion protein has become a possible therapeutic target, and the discovery of an F3-T3-specific agent would represent a significant step in the development of personalized

---

Received 23 January 2021; accepted 7 July 2021;
https://doi.org/10.1016/j.ymthe.2021.07.002.

[7] These authors contributed equally

**Correspondence:** Jian Wang, Department of Biomedicine, University of Bergen, Jonas Lies Vei 91, 5009 Bergen, Norway.
**E-mail:** jian.wang@uib.no
**Correspondence:** Chunsheng Kang, Department of Neurosurgery, Tianjin Medical University General Hospital, 154 Anshan Road, Heping District, Tianjin 300052, China.
**E-mail:** kang97061@tmu.edu.cn

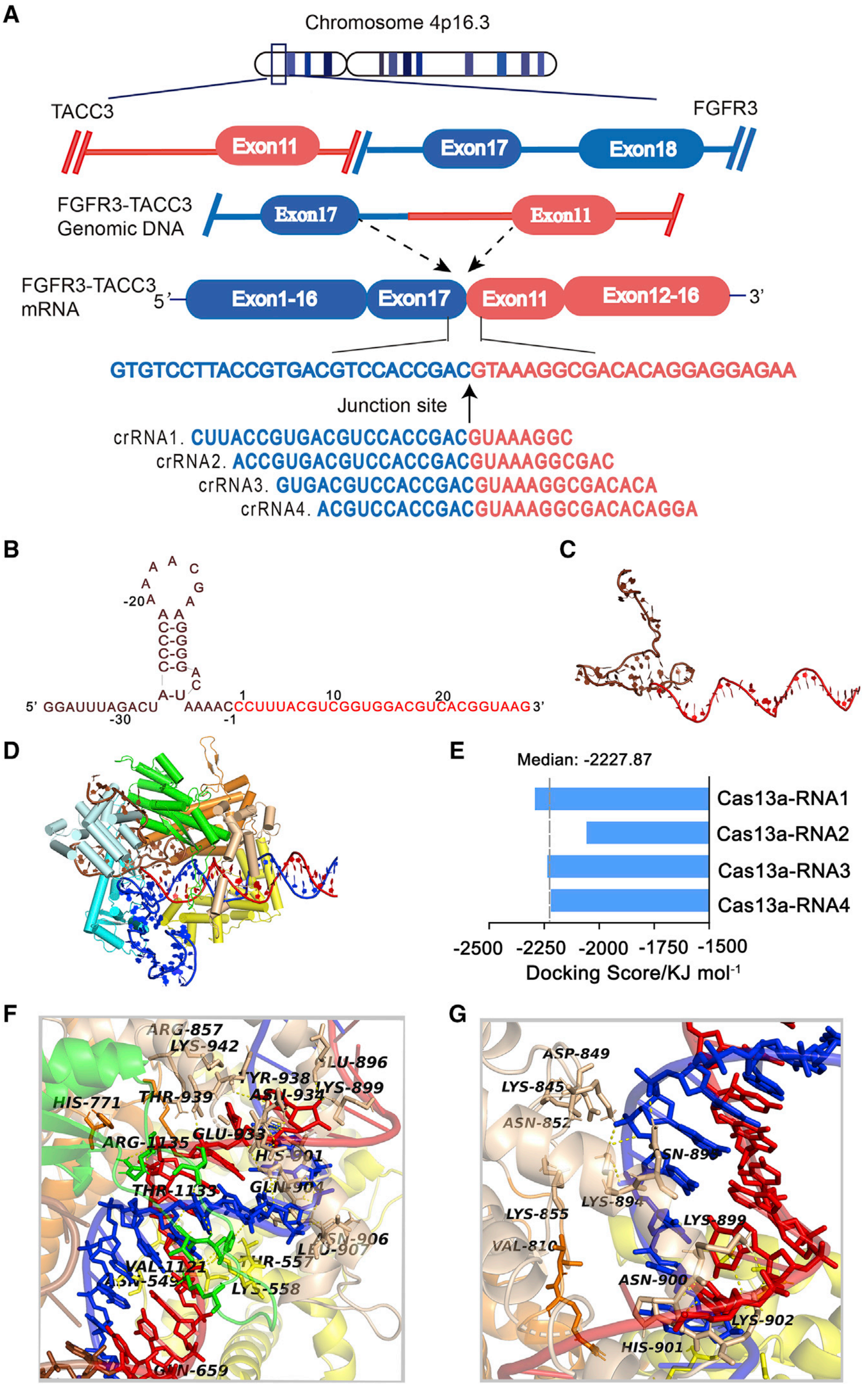

**Figure 1. Design and screen for crRNA candidates targeting FGFR3-TACC3 mRNA. (A) Scheme for the crRNA design for FGFR3-TACC3. (B) The sequences of crRNA1. Non-complementary and complementary regions within the crRNA1 are shown in brown and red, respectively. (C) Three-dimensional structure visualization of the crRNA1. (D) Structure visualization of the crRNA1-F3-T3 duplex docking to Cas13a. (E) Binding energy analysis of the Cas13a-crRNA complex. (F) Hydrogen-bond interaction of Cas13a with the bases in the 38–50 bp segment of RNA1. (G) Hydrogen-bond interaction of Cas13a with the bases in the 51–65 bp segment of RNA1**

treatment for GBM. At present, the treatment targeting FGFR3-TACC3 fusion proteins is limited to kinase inhibitors targeting FGFRs. Most of these small molecular compounds are representative multi-kinase inhibitors targeting FGFRs and other tyrosine kinases.[14] Therefore, the precise targeting of FGFR3-TACC3 would reduce adverse effects. Such a therapeutic approach could also be applied to other cancers harboring F3-T3 fusions.

Herein, we built on our previous study reporting that CRISPR-Cas13a induces a collateral effect after knocking down the target gene and kills cancer cells.[15] We found that the Cas13a system triggers a collateral effect after cleaving an F3-T3 fusion gene in human GBM cell lines, as well as other cell lines harboring F3-T3. In addition, a new computer simulation scheme was created to reduce the number of potential crRNAs requiring further confirmation. Cas13a induced a collateral effect both in cells *in vitro* and *in vivo* in an orthotopic tumor model. Our work demonstrates the value of Cas13a-based therapy targeting F3-T3 mRNA, thus confirming the CRISPR-Cas13a system as a versatile therapeutic strategy for the tailored treatment of human GBM.

## RESULTS

### Customized design and screen of potentially optimal crRNA candidates targeting FGFR3-TACC3 mRNA

In the released version of the sequence of FGFR3-TACC3, one of the most common mRNA fusion variants found in GBM, the in-frame fusion of exon 17 from FGFR3 and exon 11 from TACC3 was identified.[11] We used a tiling array to identify the junction site of F3-T3 and selected the most stable sequences among four crRNAs through *in silico* evaluation (Figure 1A). The non-complementary region (protein binding region), which contains a hairpin structure, is responsible for the stability between RNA and Cas13a. The complementary region (guide region) of the crRNA identifies the target gene through a complementary sequence that positions Cas13a for cutting the target strand. These two characteristics together ensure precise RNA cleavage by Cas13a.[6]

**Table 1. Hydrogen bond interaction analysis on F3-T3-Cas13a-cr1 complex**

| RUN | X-H…Y | Donor Atom | Acceptor Atom | Distance | Angle DHA |
|---|---|---|---|---|---|
| 1 | A:SER555:HG-B:crRNA1:G45:OP1 | HG | OP1 | 2.8 | 71.0 |
| 2 | A:SER558:2HZ-B:crRNA1:G45:OP2 | 2HZ | OP2 | 1.6 | 92.6 |
| 3 | A:SER558:1HZ-B:crRNA1:G45:OP2 | 1HZ | OP2 | 2.8 | 155.0 |
| 4 | A:HIS901:HD1-B:F3T3:C17:O2 | HD1 | O2 | 2.8 | 121.4 |
| 5 | A:GLN904:2HE2-B:F3T3:C18:O2 | 2HE2 | O2 | 2.5 | 90.3 |
| 6 | A:GLN904:2HE2-B:F3T3:G19:C4 | 2HE2 | C4 | 3.1 | 79.4 |
| 7 | A:ARG1135:2HH2-B:crRNA1:G48:OP1 | 2HH2 | OP1 | 2.5 | 121.9 |
| 8 | A:ARG1135:2HH1-B:crRNA1:G48:OP1 | 2HH1 | OP1 | 2.0 | 131.1 |
| 9 | A:LYS845:1HZ-B:F3T3:U13:OP1 | 1HZ | OP1 | 3.1 | 99.7 |

The construction of the four crRNA models is therefore divided into two steps: construction of a non-complementary region and construction of a complementary region. *In silico* calculations performed on the four crRNA candidates yielded the most suitable crRNA structure with the following characteristics. CrRNA1 (cr1) used for modeling consists of a 28 nt guide region (C1 to G28, in red) and a 37 nt protein binding region (G [−37] to C [−1], in brown) (Figure 1B). Gromacs 4.6 dynamics software was used for optimization and visualization of the three-dimensional (3D) structure of crRNA1 (Figure 1C).

The crystal structures of *Leptotrichia shahii* C2c2 in its crRNA-free and crRNA-bound states have been reported. C2c2 contains a crRNA recognition (REC) lobe and a nuclease (NUC) lobe. The REC lobe consists of an N-terminal domain (NTD) and a helical-1 domain. The NUC lobe consists of two conserved HEPN domains, with a linker connecting two HEPN domains and a helical-2 domain. The helical-1 and HEPN domains are responsible for independently cleaving pre-crRNA and target RNA, respectively.[5] The structure of the Cas13a-crRNA1 binary complex after optimization is shown Figure S1A.

Next, we performed structural prediction on the crRNA-F3-T3 binary complex. The double-stranded RNA consisting of the crRNA and the F3-T3 mRNA are referred to as the RNA. To ensure consistency in chain length and software input requirements, the length of the F3-T3 mRNA target region included was also 67 nt. Modeling and optimization in Gromacs 4.6 yielded a reasonable 3D structure of the double-stranded RNA. The guide region of crRNA1 and the F3-T3 mRNA form a 28 bp guide-target RNA complex, which resembles an A-form helix (Figure S1B). On the basis of the template 5XWP structure, the modeling double-stranded RNA was docked to Cas13a and generated the Cas13a-RNA1 ternary complex, which was visualized in PyMol version 1.60 (Figure 1D). The 28 bp guide-target RNA binary complex is located in an active channel within the NUC lobe. To compare the interactions of the four RNAs with Cas13a, the binding energies were calculated. The docking scores between RNAs and Cas13a ranged from −2,292.17 to −2,057.45 KJ/mol, with a median docking score of −2,227.87 KJ/mol (Figure 1E). The score for Cas13a-RNA1 was lower than for the other three ternary complexes, suggesting that the binding stability of Cas13a-RNA1 was relatively high and likely to lead to a greater cleavage effect.

Further study of the electrostatic binding surface of the Cas13a-RNA1 complex revealed that most regions in the active channel of Cas13a were positively charged, and the exposed oxygen atoms of RNA1 could be adequately matched with the positively charged region of Cas13a, so as to promote the binding of crRNA1 to the F3-T3 site in the mRNA and thus enhance cleavage efficiency (Figure S1C, front and side view). These findings, along with a binding energy analysis, established crRNA1 as a theoretically optimal sequence among the four crRNA candidates.

An in-depth analysis of the interactions between Cas13a, crRNA1, and F3-T3 was further performed. The crRNA1-F3-T3 duplex forms extensive contacts with Cas13a. Key residues such as Ser-555, Ser-558, His-901, Gln-904, and Arg-1135 at the active site of Cas13a exhibit strong hydrogen bond interactions with the bases in the 38–50 nt segment of RNA1, in which Ser-558, Gln-904, and Arg-1135 also form double hydrogen bond interactions with the bases (Figure 1F; Figure S1D). In addition, residue Lys-845 further forms strong hydrogen bond interactions with bases in the 51–65 nt segment of RNA1, which improves the binding stability of crRNA1 to F3-T3 and ensures the stability of cleavage (Figure 1G; Figure S1E). Analysis of crucial hydrogen bonds (containing hydrogen bond donors, acceptors, and bond length) between Cas13a and crRNA1 is shown in Table 1. Hydrogen bond interactions are spread throughout the guide region, strengthening the binding stability of RNA1 to Cas13a and enhancing the crRNA1-guided split efficiency. In brief, these analyses provide a theoretical basis for Cas13a-based RNA cleavage at the molecular level.

### CrRNA candidates attenuate expression of the F3-T3 mRNA in cultured cells

To test the cleavage efficiency of the crRNAs, functional experiments were performed *in vitro* in cells expressing an F3-T3 mRNA. U87 and

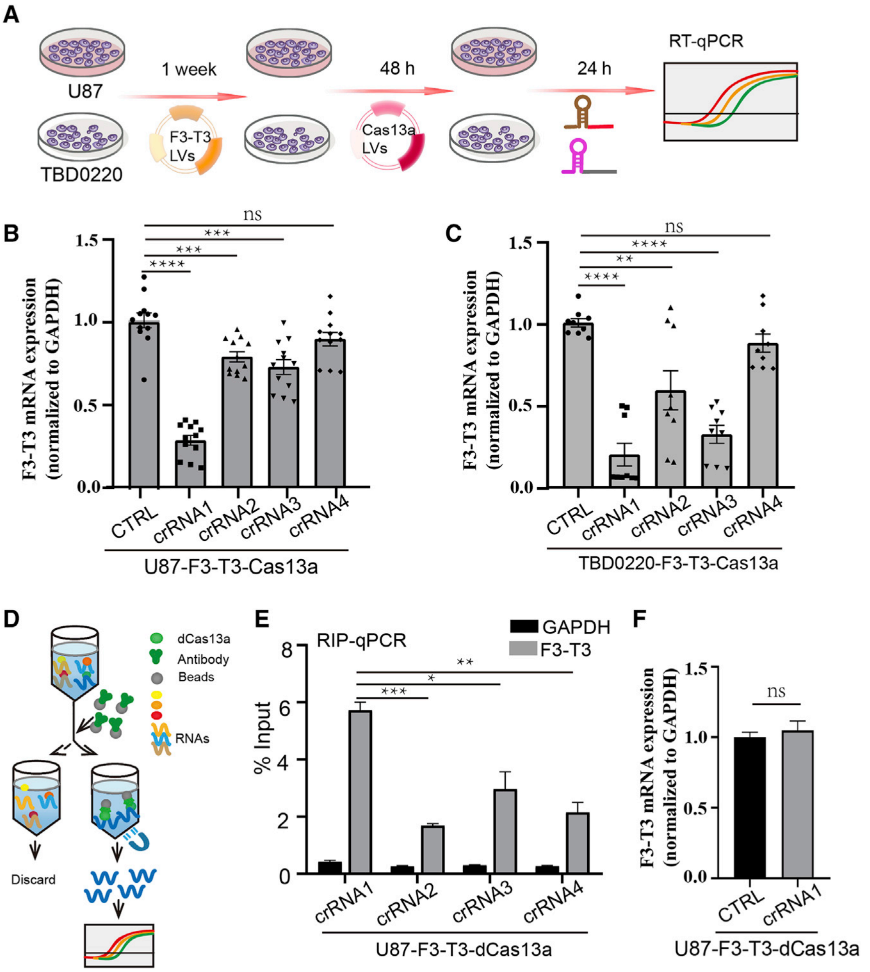

**Figure 2. Confirmation of the efficiency of crRNA candidates. (A) Schematic diagram of the transfection process in U87 and TBD0220 cells for subsequent assays. (B and C) qRT-PCR analysis to examine F3-T3 mRNA at 24 h in U87-F3-T3-Cas13a and TBD0220-F3-T3-Cas13a cells transfected with a non-targeting crRNA and the four crRNAs. Bars represent mean ± SEM (n = 9). **p < 0.01, ***p < 0.001, and ****p < 0.0001; ns, p > 0.05. (D) Schematic diagram of the RIP experiment performed in U87 cells with a dead Cas13a (dCas13a) and the four different crRNAs. (E) RIP-qPCR to examine the binding efficiency of each of the four crRNA candidates at 24 h after transfection with Lipofectamine. The negative control was GAPDH. *p < 0.05, **p < 0.01, and ***p < 0.001. (F) qRT-PCR analysis to examine F3-T3 expression levels when Cas13a is replaced with a dead Cas13a (dCas13a). ns, p > 0.05**

TBD0220 cells were infected with a lentivirus expressing the F3-T3 mRNA. After 1 week in selection with puromycin, the cells were infected with a second lentivirus expressing Cas13a for at least 48 h. The four crRNAs targeting the F3-T3 mRNA were then transfected into the resultant cell populations, U87-F3-T3-Cas13a and TBD0220-F3-T3-Cas13a, with Lipofectamine 3000, and the levels of the F3-T3 mRNA were determined using qRT-PCR (Figure 2A). On the basis of Ct values normalized to *GAPDH*, crRNA1 exhibited the most significant knockdown efficiency compared with the control non-targeting crRNAs (Figures 2B and 2C). Similarly, crRNA1-mediated loss of F3-T3 mRNA levels was observed in N9, PC9, MDA-MB-231, and A375 cells (Figure S2).

Catalytically inactive LwaCas13a (dCas13a) maintains targeted RNA binding activity but not cleavage activity.[16] Labeled RNA has been applied to the dCas13 system, allowing visualization of the position and dynamics of RNAs with the protein in live cells.[17] To further examine binding stability, we performed RNA-binding protein immunoprecipitation (RIP)-qPCR on RNA obtained from complexes in U87 cells infected with a dCas13a expressing lentivirus (U87-F3-T3-dCas13a) and transfected with crRNAs for 24 h (Figure 2D). The RIP-qPCR analyses indicated that F3-T3 exhibited the highest enrichment in crRNA1-transfected cells (Figure 2E). Taken together, these data suggested that crRNA1 has the highest binding stability and thus the most significant impact on knockdown of the F3-T3 mRNA. These results were consistent with the molecular structure simulation. In contrast, crRNA1 transfection into U87-F3-T3-dCas13a cells did not lead to knockdown of F3-T3 mRNA (Figure 2F). These data indicated that crRNA1-guided CRISPR-Cas13a could lead to robust depletion of F3-T3 mRNA in cells through specific targeting of F3-T3 fusion breakpoints.

## Collateral RNA damage induced by Cas13a-cr1 requires the presence of F3-T3 mRNA *in vitro*

To determine whether the specific cleavage of F3-T3 mRNA triggered the overall degradation of RNA in glioma cells, the so-called collateral RNA damage, we examined the integrity of ribosomal and gene specific RNAs in U87-F3-T3-Cas13a cells transfected with cr1. Total RNA collected at different time points after transfection of cells with cr1 exhibited degradation starting at 24 h as assessed on denaturing RNA gels (Figure 3A). In contrast, the transfection of cr1 into U87-Cas13a cells without F3-T3 did not cause ribosomal RNA degradation (Figure 3B).

The integrity of total RNA, as assessed using the Agilent Bioanalyzer (Figure 3C), from U87-F3-T3-Cas13a cells after cr1 transfection at 24 h was destroyed, while that in U87-Cas13a cells remained intact (Figure 3D). The ratio of 28S to 18S ribosomal bands was also decreased in U87-F3-T3-Cas13a-cr1 cells (Figure 3D). Experiments

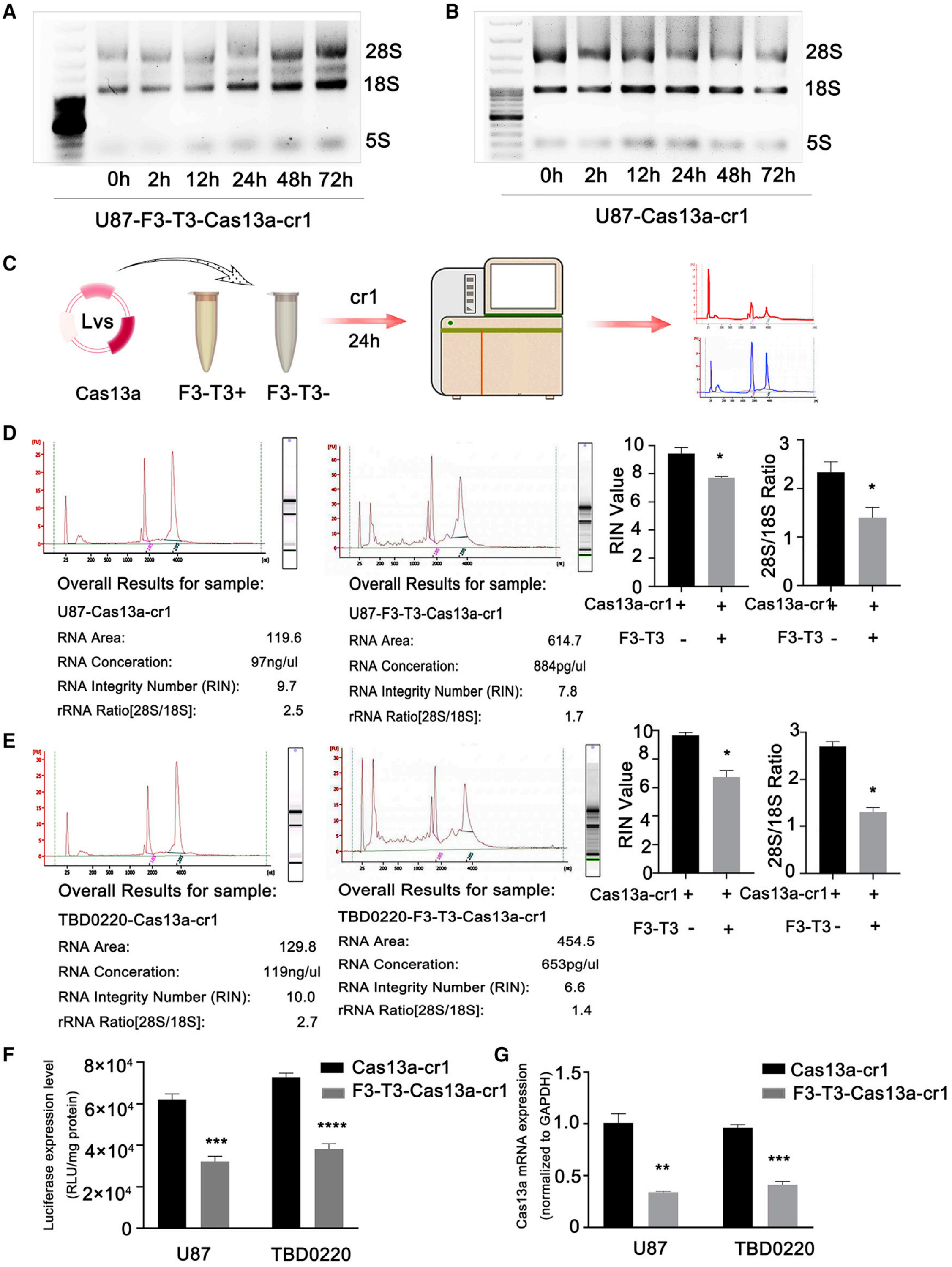

Overall Results for sample:
U87-Cas13a-cr1
RNA Area: 119.6
RNA Conceration: 97ng/ul
RNA Integrity Number (RIN): 9.7
rRNA Ratio[28S/18S]: 2.5

Overall Results for sample:
U87-F3-T3-Cas13a-cr1
RNA Area: 614.7
RNA Conceration: 884pg/ul
RNA Integrity Number (RIN): 7.8
rRNA Ratio[28S/18S]: 1.7

Overall Results for sample:
TBD0220-Cas13a-cr1
RNA Area: 129.8
RNA Conceration: 119ng/ul
RNA Integrity Number (RIN): 10.0
rRNA Ratio[28S/18S]: 2.7

Overall Results for sample:
TBD0220-F3-T3-Cas13a-cr1
RNA Area: 454.5
RNA Conceration: 653pg/ul
RNA Integrity Number (RIN): 6.6
rRNA Ratio[28S/18S]: 1.4

*(legend on next page)*

performed with the Cas13a-based tool in other cell lines yielded similar results (Figure 3E; Figure S3A).

Next, we transfected luciferase reporter genes into the two cell lines and assessed whether there was comprehensive RNA degradation on the basis of the loss of luciferase activity 24 h after transfection of cr1. Luciferase activity decreased by almost 50% in the F3-T3-containing cells compared with the activity in F3-T3-negative cells (Figure 3F). Finally, Cas13a mRNA levels were also significantly decreased only in the F3-T3-positive groups (Figure 3G). The expression of two random, intrinsically expressed RNAs, *HOTAIR* and *L3MBTL1*, also decreased by ∼50% in several cells lines expressing Cas13a and F3-T3 and transfected with cr1 (Figure S3B). In this context, these results indicated that Cas13a exhibited no detectable off-target effects and might trigger collateral effects after precisely targeting the F3-T3 mRNA.

### Cas13a-based tool causes loss of F3-T3-induced expression in U87 cells

To further explore the collateral and functional effects of the Cas13a-based strategy, we examined RNA integrity and global expression in modified or AZD4547-treated U87 cells on the Agilent Human ceRNA Microarray 2019 (4*180k, Design ID: 086188). First, we examined RNA degradation in U87-F3-T3-Cas13a-cr1 cells and U87-F3-T3 cells treated with AZD4547 for 24 h (a selective FGFR1-3 tyrosine kinase inhibitor) at two-thirds of the half maximal inhibitory concentration ($IC_{50}$) (Figure S4). Consistent with previous results, the collateral effect was detected in U87-F3-T3-Cas13a-cr1 cells only (Figures 4A–4C).

Pearson's correlation analysis of the microarray data showed a low correlation between U87-F3-T3-Cas13a-cr1 cells and both U87-F3-T3 and U87-F3-T3-AZD4547 cells (Figure 4D). A heatmap generated from cluster analysis performed on differentially expressed genes from the four groups of cells, including control and AZD4547-treated cells, revealed that genes induced by F3-T3 were lost in U87-F3-T3-Cas13a-cr1 cells. In marked contrast, AZD4547 was not as effective in suppressing the downstream transcription effects of F3-T3 in U87 cells (Figure 4E). The data were further analyzed using gene set variation analysis (GSVA), which revealed that malignant biological processes (including immune response-related signatures and apoptosis) and oncogenic pathways (including the KRAS and mTOR signaling pathways) were enriched in U87-F3-T3-Cas13a-cr1 cells. This result was similar to our previous results, which might be related to the cellular response due to gene-editing stress.[15] However, cell cycle-related terms (including Myc targets and E2F targets) were suppressed in U87-F3-T3-Cas13a-cr1 cells and U87-F3-T3-AZD4547 cells (Figure 4F). In summary, these results indicated that the Cas13a-based tool reversed some of the mRNA changes induced by F3-T3 overexpression and was more effective than AZD4547, a traditional inhibitor of F3-T3 fusion proteins.

### Cas13a-cr1 inhibits F3-T3 overexpression-induced cell proliferation and induces apoptosis *in vitro*

To further probe the functional consequences of targeting the F3-T3 fusion gene with the Cas13a-based tool, we examined protein expression of F3-T3 and cell proliferation. Immunofluorescence assays showed that cr1 significantly inhibited F3-T3 expression in U87-F3-T3-Cas13a-cr1 or TBD0220-F3-T3-Cas13a-cr1 cells relative to U87-F3-T3 or TBD0220-F3-T3 cells (Figures S5A and S5B). In colony formation and CCK-8 assays, U87 and TBD0220 cells overexpressing F3-T3 exhibited increased proliferation compared with control groups. In contrast, colony numbers and cell proliferation were dramatically decreased in U87- and TBD0220-F3-T3-Cas13a-cr1 cells compared with U87- and TBD0220-F3-T3 and AZD4547-treated cells or controls (Figures 5A–5D). Cas13a-cr1-induced inhibitory effects were also observed in N9, PC-9, MDA-MB-231, and A375-F3-T3 cells (Figures S5C–S5E). Furthermore, flow cytometry revealed a significant increase in the percentage of U87- and TBD0220-F3-T3-Cas13a-cr1 cells in G0/G1 compared with U87 and TBD0220-F3-T3 cells ($p < 0.0001$ and $p < 0.001$; Figures 5E–5G), while the increase in the percentage of AZD4547-treated cells in G0/G1 was more modest ($p < 0.01$; Figures 5E–5G). Immunoblotting also revealed lower protein expression of CDK4, CDK6, and cyclin D1 in Cas13a-cr1-treated cells compared with U87 and TBD0220-F3-T3 cells and AZD547-treated cells (Figure 5H). The percentage of U87- and TBD0220-F3-T3-Cas13a-cr1 cells undergoing apoptosis also increased to a greater extent than for AZD4547-treated cells compared with U87 and TBD0220-F3-T3 cells (Figures 5I–5K). In addition, the expression of proteins involved in apoptosis, caspase-3 and caspase-7,[18] increased in the presence of Cas13a-cr1 (Figure 5L). Thus, these data indicated that Cas13a-cr1 efficiently inhibited proliferation and induced apoptosis in tumor cells in culture harboring the F3-T3 fusion gene.

### The Cas13a-based tool induces efficient tumor regression *in vivo*

We also examined the ability of the Cas13a-based tool or AZD4547 to inhibit U87-F3-T3 tumor growth in an intracranial GBM model in BALB/c nude mice (Figure 6A). Tumors for all four cell types were detectable by day 7. Luminescence detected from U87-F3-T3 tumors was, however, greater than for control tumors and continued to increase over the course of 21 days ($p < 0.0001$). In contrast, U87-F3-T3-Cas13a-cr1 tumors grew more slowly over the course of 21 days compared with U87-F3-T3 tumors ($p < 0.0001$). Treatment of animals with AZD4547

**Figure 3. Cas13a-cr1 induces a collateral effect in glioma cells. (A and B) RNA-denaturing gel electrophoresis of total RNA from U87-F3-T3-Cas13a and U87-Cas13a cells transfected with cr1 and collected at different time points to assess RNA integrity. (C) Schematic diagram of the workflow for RNA quality control. (D and E) Analysis of RNA quality performed on the Agilent 2100 Bioanalyzer. Bars represent mean ± SEM (n = 3). *$p < 0.05$. (F) Bioluminescence of luciferase reporter genes expressed in U87- and TBD0220-Cas13a or -F3-T3-Cas13a cells after transfection of cr1. The results are represented as RLU/mg protein. Bars represent mean ± SEM (n = 3). ***$p < 0.001$ and ****$p < 0.0001$. (G) qRT-PCR analysis to examine Cas13a mRNA levels in U87- and TBD0220-Cas13a and -F3-T3-Cas13a cells after transfection of cr1 at 24 h. Bars represent mean ± SEM (n = 3). **$p < 0.01$ and ***$p < 0.001$**

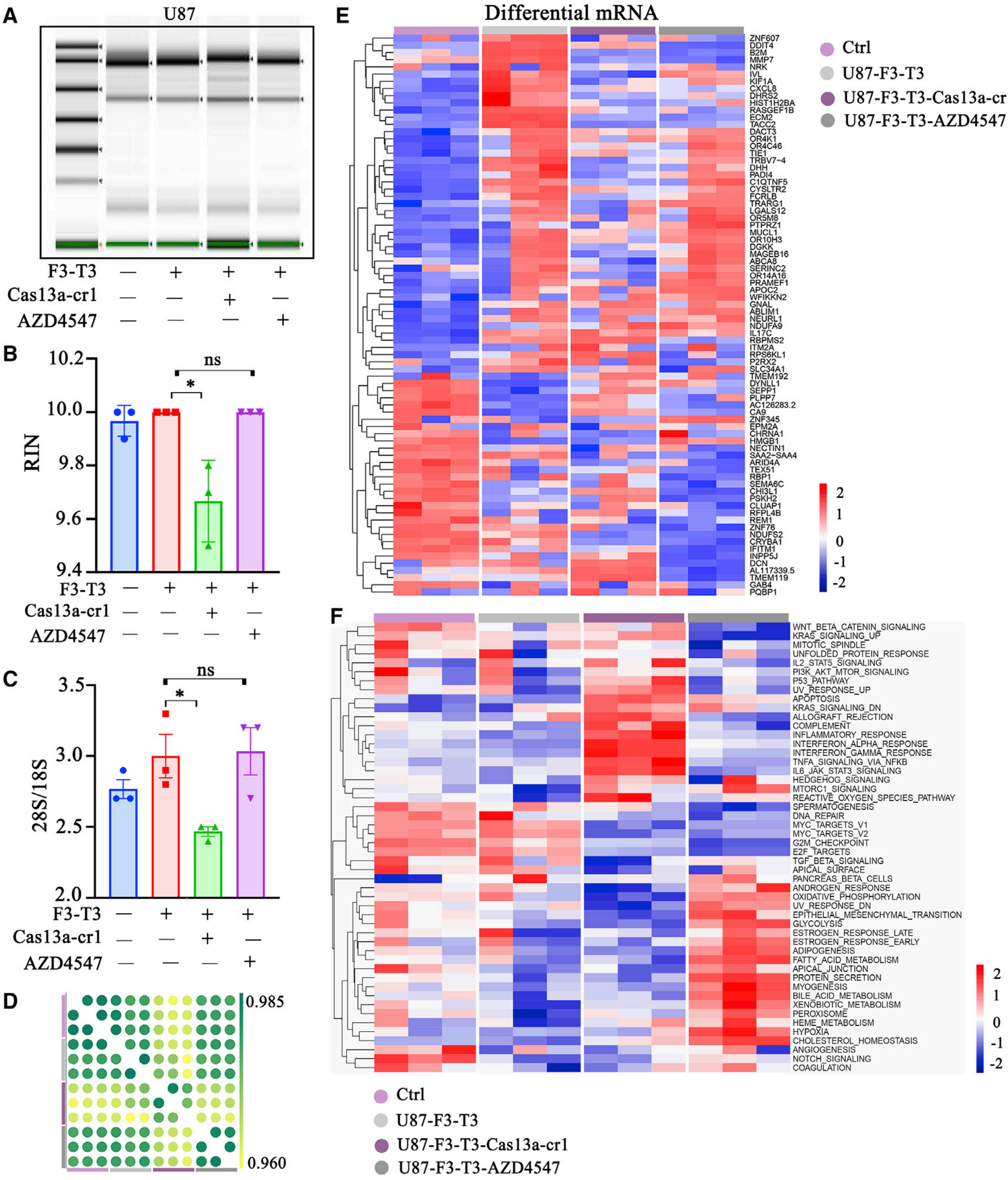

**Figure 4. Profile of the collateral effect induced by the Cas13a-cr1 based tool. (A) Electrophoretogram of total RNA isolated from the cell populations indicated. (B and C) RNA integrity number (RIN) and the ratio of 28S to 18S as determined on the Agilent 2100 Bioanalyzer for the cell populations indicated. ns, $p > 0.05$. *$p < 0.05$. (D) Pearson correlation analysis of RNA expression in the cell populations indicated. (E) Heatmap of differentially expressed mRNA from the four types of cells on the basis of microarray analysis. (F) Heatmap of the GSVA analysis of the four groups. The rows represent the 50 hallmark gene sets. Three RNA samples were isolated for each cell type**

also led to a modest inhibition of U87-F3-T3 tumor growth compared with untreated U87-F3-T3 tumors in mice ($p < 0.01$; Figures 6B and 6C). Kaplan-Meier survival curves demonstrated that the U87-F3-T3 tumor-bearing mice exhibited poorer overall survival compared with control animals ($p < 0.001$). U87-F3-T3-Cas13a-cr1 tumor-bearing mice showed improved overall survival compared with untreated U87-F3-T3 tumor-bearing mice ($p < 0.001$; Figure 6D). However, U87-F3-T3 tumor-bearing mice treated with AZD4547 showed only a slight improvement in overall survival compared with untreated U87-F3-T3 tumor-bearing mice ($p < 0.05$; Figure 6D). The body weight of

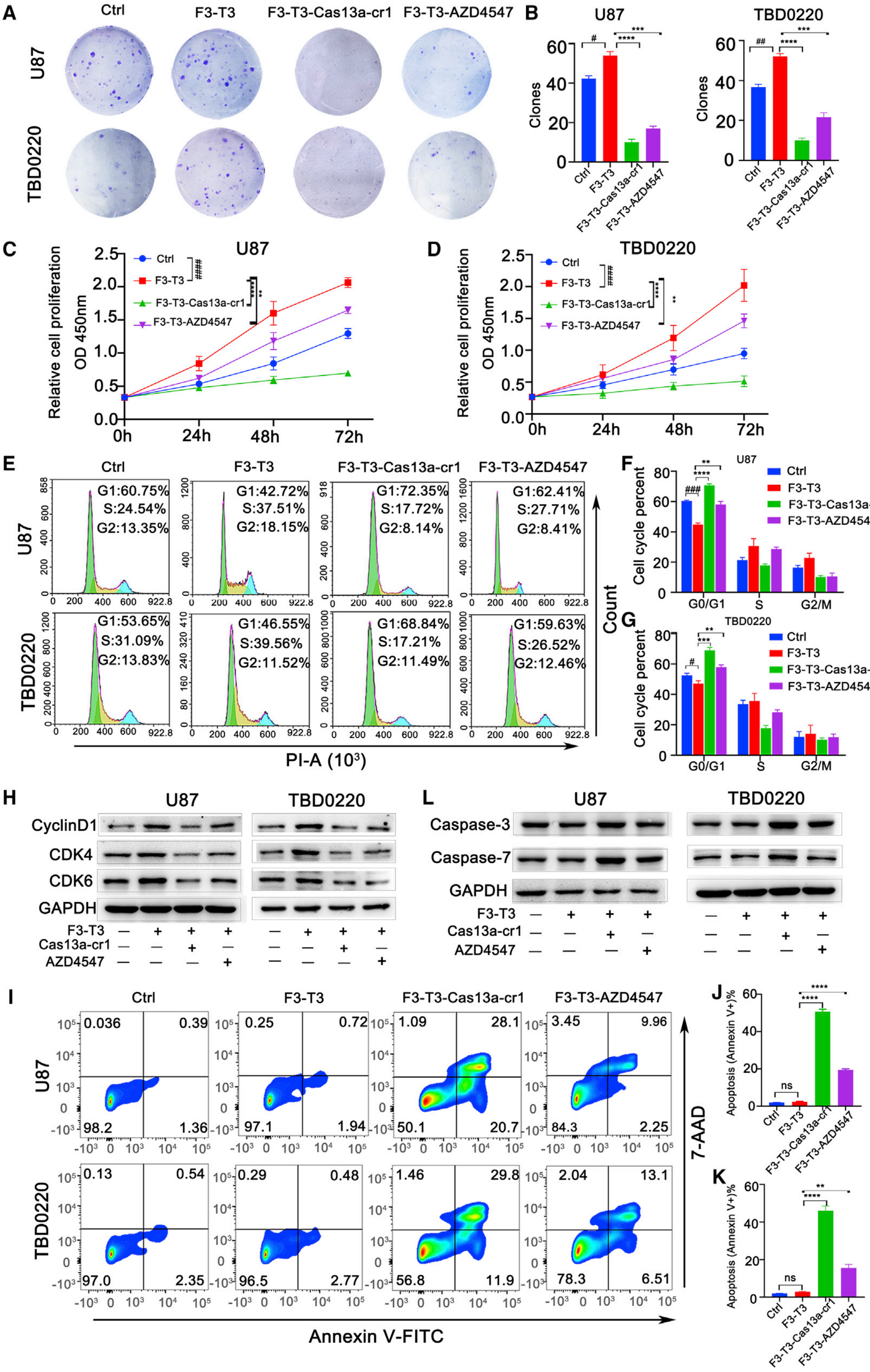

*(legend on next page)*

U87-F3-T3 tumor-bearing mice also decreased more rapidly than in control animals ($p < 0.0001$) or in U87-F3-T3-Cas13a-cr1 tumor-bearing animals ($p < 0.0001$; Figure 6E) after day 7 post-implantation.

H&E staining confirmed the smaller size of the U87-F3-T3-Cas13a-cr1 tumors relative to U87-F3-T3 tumors or U87-F3-T3 tumors treated with AZD4547 (Figure 6F). Ki67 staining also revealed a higher percentage of proliferating cells in U87-F3-T3 tumors compared with U87-F3-T3-Cas13a-cr1 ($p < 0.0001$) or control tumors ($p < 0.0001$). However, Ki67 staining revealed only a modest inhibition of growth in AZD4547-treated U87-F3-T3 tumors ($p < 0.05$; Figures 6G and 6H). We surprisingly found that the Cas13a-based therapy outperformed treatment with a traditional selective FGFR-TK inhibitor AZD4547 on the basis of all estimated parameters, illuminating its potential as a novel strategy for the treatment of tumors harboring F3-T3 fusion genes.

### Intratumoral delivery of Cas13a system with mini-osmotic pump

We also examined the efficacy of intracranial delivery of the CRISPR-Cas13a system directly into gliomas. PEI-PBLG (PP) was used as the delivery vehicle for CRISPR-Cas13a system, and the complex was delivered directly into intracranial tumors using the Alzet mini-osmotic pump, which is an efficient approach for intratumoral administration circumventing the blood-brain barrier (Figure 7A).[19] PP condensed plasmid DNA (pDNA) efficiently at low (wt/wt) ratios, and at a [carrier]/[DNA] (wt/wt) ratio of 1, PP completely complexed with the DNA. The average diameter of the complex particles was about 100 nm, which is reported to be a particle size favorable for effective endocytosis (Figure S6).[20] Treatment of animals with Cas13a-cr1 led to a significant reduction in U87-F3-T3 tumor growth in mice compared with vehicle control groups. In contrast, delivery of Cas13a or cr1 alone did not lead to a reduction in U87-F3-T3 tumor growth in mice compared with the vehicle control groups ($p < 0.00001$; Figures 7B and 7C). Kaplan-Meier survival curves demonstrated that Cas13a-cr1-treated tumor-bearing mice showed improved overall survival compared with the vehicle control mice ($p < 0.0001$; Figure 7D). Delivery of Cas13a or cr1 alone also did not improve overall survival over the vehicle control mice ($p > 0.05$; Figure 7D). The body weight of vehicle control mice decreased more rapidly than in Cas13a-cr1-treated mice after day 7 post-implantation ($p < 0.0001$; Figure 7E). H&E staining confirmed the smaller size of the Cas13a-cr1-treated tumors relative to vehicle control tumors. However, delivery of Cas13a or cr1 alone into tumors did not reduce tumor size compared with vehicle control (Figure 7F). Ki67 staining also revealed a lower percentage of proliferating cells in Cas13a-cr1-treated tumors compared with vehicle control tumors ($p < 0.0001$). Cas13a or cr1 treatment alone, however, did not lead to a reduced percentage of proliferating cells ($p > 0.05$; Figures 7G and 7H). These data suggested that Cas13a-based therapy potently inhibited tumor growth, thus providing evidence for its potential as a promising strategy for the treatment of tumors harboring F3-T3 fusion genes.

## DISCUSSION

Here, we used a tiling array to identify the junction site of the fusion F3-T3 mRNA and designed a computer simulation scheme to choose optimal crRNA candidates specifically and efficiently. The stability of the crRNA-Cas13a complex was determined through docking scores generated in our analysis, and cr1 was found to be the most optimal candidate. Subsequently, the targeting efficiency of cr1 was evaluated in cancer cells expressing F3-T3 mRNA. The Cas13a-based tool caused a loss of RNA integrity and a change in gene expression only in cells expressing the F3-T3 mRNA. In an orthotopic xenograft mouse model, we further demonstrated the therapeutic potential of Cas13a-cr1.

Highly potent and sensitive FGFR-TK inhibitors have been published over the past decade, and some are in clinical trials, such as ADZ4547 and BGJ398.[11,21,22] However, despite the specific targeting of the kinase portion of FGFR, the incidence of significant side effects and accelerated growth of drug resistant cells are major drawbacks for effective treatment with kinase inhibitors in the clinic.[23] Even though expression levels of wild-type FGFR3 are low in normal brain, the receptor exists in several peripheral organs, and consequently, methods targeting the kinase domain of FGFR may result in normal tissue toxicity.[24] AZD4547 is a multi-kinase inhibitor that targets FGFRs and other tyrosine kinases.[14] Oral inhibitors are a method of systemic administration, rendering the adverse effects caused by off-target effects as the main obstacle to anti-cancer treatment.[25] In contrast, CRISPR-Cas13a-based therapeutic strategies exhibit tumor specificity. In our study, we demonstrated the killing capacity of CRISPR-Cas13a-based in targeting an F3-T3-positive glioma upon recognition of F3-T3 mRNA under the guidance of crRNA. This strategy may be of benefit to patients with F3-T3-positive tumors, which currently lack any valuable therapeutic options.

Although the CRISPR-Cas13a system has opened up a wide range of therapeutic possibilities, delivery is among the most compelling

**Figure 5. Cas13a-based tool inhibits cell proliferation and induces apoptosis *in vitro*. (A) Images of colony formation assays performed in U87 and TBD0220 cells: control, -F3-T3, -F3-T3-Cas13a-cr1, and F3-T3-AZD4547. (B) Quantification of colony numbers in (A). #$p < 0.05$ and ##$p < 0.01$ versus the control group; ***$p < 0.001$ and ****$p < 0.0001$ versus the F3-T3 group. (C and D) Growth curves generated with CCK8 assays to analyze the proliferation of U87 and TBD0220 cells. ####$p < 0.0001$ versus the control group; **$p < 0.01$ and ****$p < 0.0001$ versus the F3-T3 group. (E) Cell cycle analysis on the basis of PI staining and fluorescence-activated cell sorting (FACS) performed after exposure of U87 and TBD0220 cells to indicated treatment for 48 h. (F and G) Graphic representation of the distribution of cells in each cell cycle phase in (E). #$p < 0.05$ and ###$p < 0.001$ versus the control group; **$p < 0.01$, ***$p < 0.001$, and ****$p < 0.0001$ versus the F3-T3 group. (H) Immunoblotting analysis of CDK4, CDK6, and cyclin D1 after exposure of cells with indicated treatment for 48 h. (I) Flow cytometry of Annexin V-FITC and 7-AAD staining of U87 and TBD0220 cells after indicated treatment for 48 h. (J and K) Apoptosis percentage from (I). ns, $p > 0.05$. **$p < 0.01$, ***$p < 0.001$, and ****$p < 0.0001$ versus the F3-T3 group. (L) Immunoblotting analysis of caspase-3 and caspase-7 in cells under indicated treatment for 48 h**

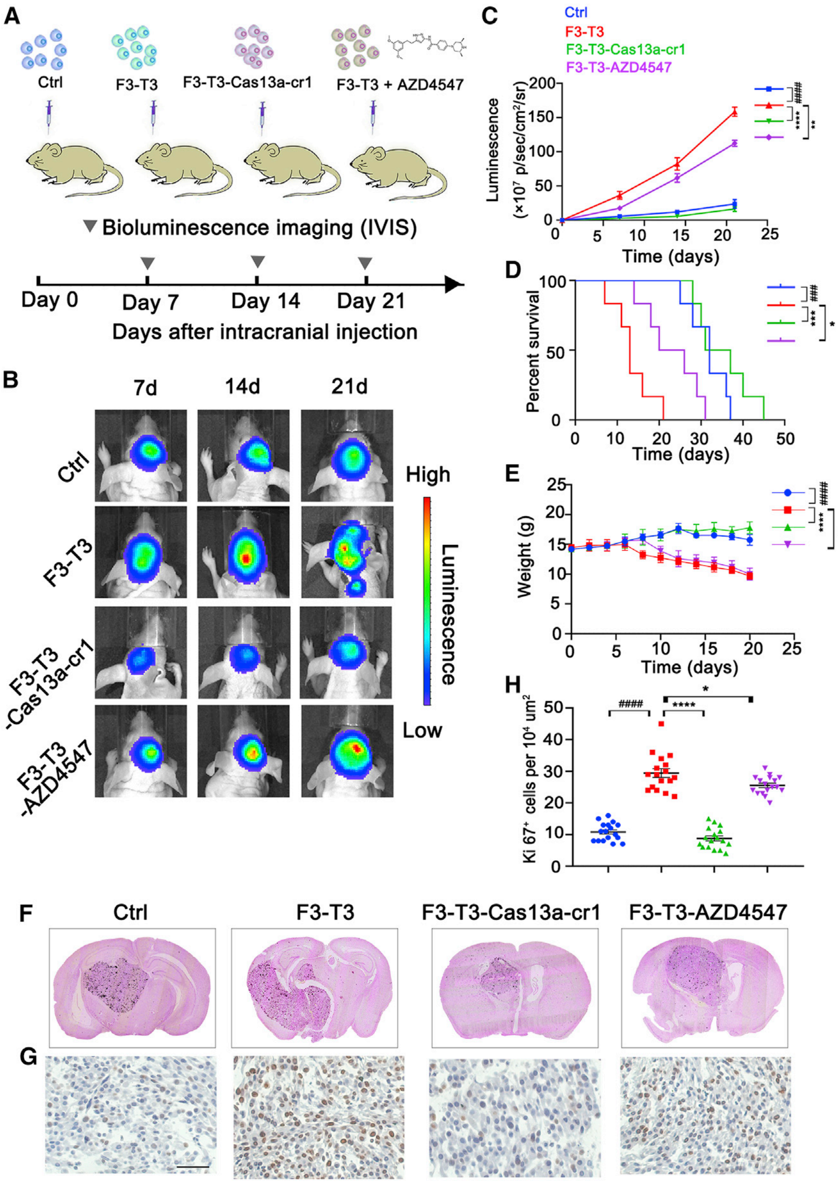

**Figure 6. Cas13a-based tool inhibits the formation of intracranial tumors. (A) Schematic of experimental grouping and processing of the orthotopic xenograft model. Oral administration of AZD4547 (50 mg/kg) was performed daily in the U87-F3-T3-AZD4547 group. (B and C) Bioluminescence imaging of tumor growth in animals. Signal intensities were quantified at days 7, 14, and 21 after implantation. n = 6 per group. ####$p < 0.0001$ versus the control group; **$p < 0.01$ and ****$p < 0.0001$ versus the F3-T3 group. (D) Kaplan-Meier survival curves indicating the percentage survival of mice. ###$p < 0.001$ versus the control group; *$p < 0.05$ and ***$p < 0.001$ versus the F3-T3 group; log rank test. (E) Graphic representation of weight of animals over time. n = 6 for each group. ####$p < 0.0001$ versus the control group; ****$p < 0.0001$ versus the F3-T3 group. ns, $p > 0.05$. (F) Representative images of H&E staining of mouse cerebrum showing tumor volume. (G) Immunohistochemical (IHC) staining for Ki67 in the samples. Scale bar, 50 μm. (H) Quantification of Ki67 was performed using ImageJ software for each high-magnification view. n = 6 per group. Scale, 50 μm. ####$p < 0.0001$ versus the control group. *$p < 0.05$ and ****$p < 0.0001$ versus the F3-T3 group**

obstacles in the application of this system. Generally, there are two major delivery methods: non-viral and viral.[26] For non-viral methods, there are lipid-assisted nanoparticles, macromolecules, and designed peptides. In a previous study, we reported a multistage delivery nanoparticle that penetrates multiple physiological barriers and efficiently facilitates CRISPR-dCas9 suppression of tumor growth *in vivo*.[27] In this study, PP was used as the delivery vehicle for the CRISPR-Cas13a system, and the complex was delivered directly into the intracranial tumor using mini-osmotic pumps. Viral methods include lentivirus, adenovirus, and adeno-associated virus (AAV). Use of an AAV offers advantages not possible with lentiviruses or adenoviruses.[28] AAV vectors are the most successful delivery system currently in use and the only delivery carrier approved for the application of CRISPR therapeutics directly into the human body.[29] However, the development of an AAV-CRISPR toolbox also faces some challenges, including the high manufacturing cost, vehicle quality control, and immunological barriers.[30]

The collateral effect should be a nonspecific RNase activity triggered under specific conditions. However, some groups did not observe the collateral effect with Cas13a in human cells.[16] Several differences in this study may account for this disparity. First, they used a plasmid vector to express the Cas13a gene and crRNAs in human cancer cells, while we transfected cells with a lentivirus containing LwCas13a and then transfected crRNAs into cells using Lipofectamine 3000. Second, the knockdown efficiency of LwaCas13a was estimated on the basis of endogenous transcripts, while we used overexpression of FGFR3-TACC3 with lentivirus. Third, the human cancer cell lines in their study are HEK293FT and A375 (melanoma), while we mainly used GBM cell lines U87 and TBD0220. In another study, purified LwaCas13a protein and crRNAs were co-transfected into pancreatic cancer cells for targeted knockdown of mutant KRAS, but with no detectable collateral damage effect.[31] Further study is therefore necessary to clarify the mechanisms underlying the induction of the collateral damage effect.

With the simplicity and versatility of crRNA programming, our work demonstrates that the Cas13a system might revolutionize precision

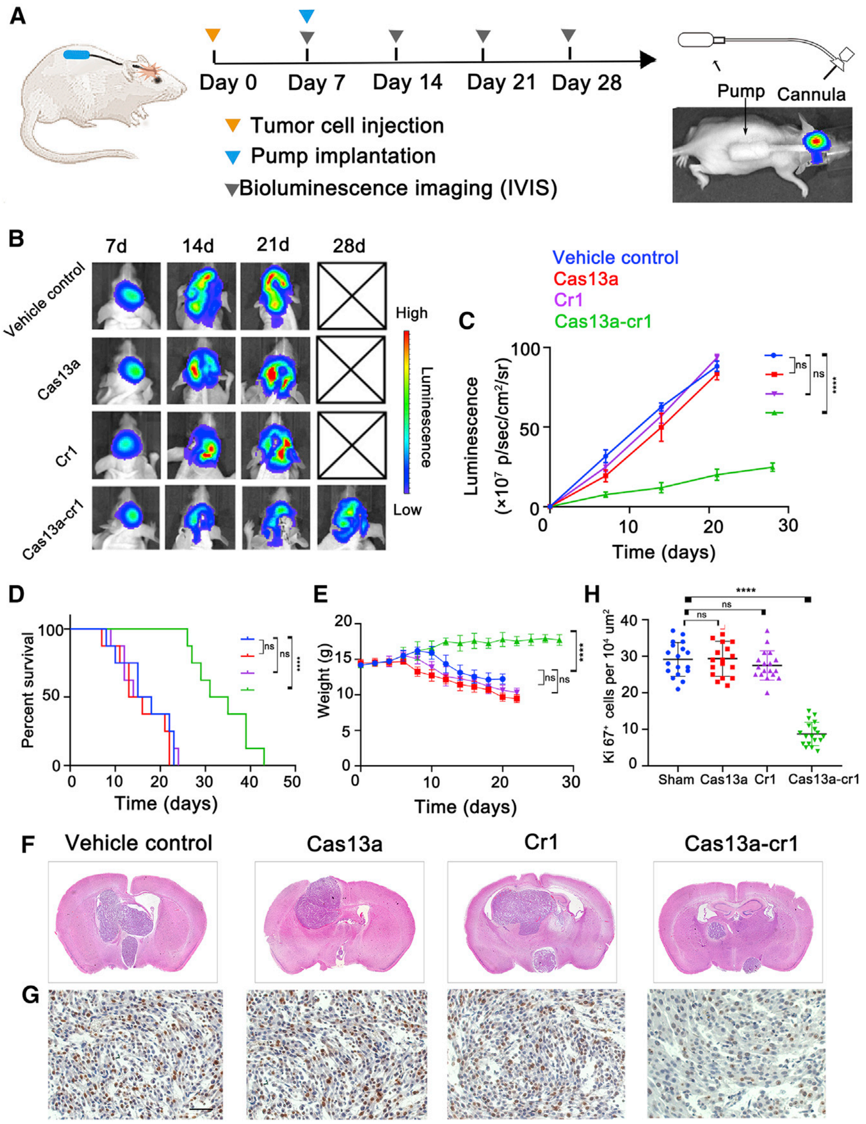

**Figure 7. Intratumoral delivery of Cas13a system inhibits growth of intracranial U87-F3-T3 tumors. (A) Schematic of experimental grouping, processing of the orthotopic xenograft model, and implantation of Alzet mini-osmotic pumps. (B and C) Bioluminescence imaging of tumor growth in animals. Signal intensities were quantified at days 7, 14, and 21 after implantation. n = 8 per group. ns, $p > 0.05$; ****$p < 0.0001$ versus the vehicle control group. (D) Kaplan-Meier survival curves indicating the percentage survival of mice. ns, $p > 0.05$; ****$p < 0.0001$ versus the vehicle control group; log rank test. (E) Graphic representation of weight of animals over time. n = 8 for each group. ns, $p > 0.05$; ****$p < 0.0001$ versus the sham group. (F) Representative images of H&E staining of mouse cerebrum showing tumor volume. (G) IHC staining for Ki67 in the samples. Scale bar, 50 μm. (H) Quantification of Ki67 was performed using ImageJ software for each high-magnification view. n = 8 per group. Scale, 50 μm. ns, $p > 0.05$; ****$p < 0.0001$ versus the sham group**

therapy in tumors harboring oncogenic fusion genes. The discussed therapeutic modalities for the improvement of CRISPR-based biotechnologies for GBM can also serve as a model for the use of this system in solid tumor cancer treatment. In conclusion, we demonstrated that the promiscuous RNA cleavage ability of the CRISPR-Cas13a system triggered by the recognition of the F3-T3 fusion gene in the presence of a specific crRNA resulted in suppression of tumor growth.

## MATERIALS AND METHODS

### Ethics statement

All *in vivo* studies were performed in compliance with animal procedures accepted by the Animal Ethical and Welfare Committee (AEWC) at the Tianjin Medical University (approval no. IRB2020-DW-16).

### Cell culture, lentivirus, and compounds

Human GBM U87 and malignant melanoma A375 cell lines were maintained in Dulbecco's modified Eagle's medium (DMEM; GIBCO) supplemented with 10% fetal bovine serum (FBS; Hakata, China). Primary cell lines N9 and TBD0220 were cultured in DMEM/F12 with 10% FBS. MDA-MB-231 (breast cancer) and PC9 (NSCLC) cell lines were cultured in RPMI 1640 medium with 10% FBS. All cells were incubated at 37°C in a humidified chamber containing 95% air and 5% $CO_2$. LwCas13a, nuclease-dead LwCas13a, and FGFR3-TACC3 lentiviruses were purchased from GENECHEM (Shanghai, China). F3-T3-positive cells were selected in puromycin (4 μg/mL for selection, 2 μg/mL for maintenance) and then transfected with Cas13a for at least 48 h, following the manufacturer's instructions. Transfected cells were used in experiments for only less than 1 month to avoid loss of the target gene. Cells ($30 \times 10^4$ cells per six-well plate) were seeded 24 h before treatment with AZD4547 (Selleck, Shanghai, China) at a concentration of two-thirds of the $IC_{50}$. (All cells were seeded 24 h before exposure to treatment.)

### CrRNA design and crRNA transfection

The crRNAs, synthesized *ex vivo* by Integrated Biotech Solutions (Shanghai, China), were designed with the CRISPR-RT Design Tool (http://bioinfolab.miamioh.edu/CRISPR-RT). Non-targeting guide sequences were obtained from previously published studies.[15] CrRNAs (300 ng/mL) were transfected with Lipofectamine R3000 (Invitrogen, Carlsbad, CA), following the manufacturer's protocol. The sequences of crRNAs were the following:

Non-targeting crRNA: 5′-CAGACUAUGCGUCGACAAGCCAGGCAUU-3′

crRNA1: 5′-GGAUUUAGACUACCCCAAAAACGAAGGGGACUAAAACCCUUUACGUCGGUGGACGUCACGGUAAG-3′

crRNA2: 5′-GGAUUUAGACUACCCCAAAAACGAAGGGGACUAAAACUCGCCUUUACGUCGGUGGACGUCACGGU-3′

crRNA3: 5′-GGAUUUAGACUACCCCAAAAACGAAGGGGACUAAAACGUGUCGCCUUUACGUCGGUGGACGUCAC-3′

crRNA4: 5′-GGAUUUAGACUACCCCAAAAACGAAGGGGACUAAAACCCUGUGUCGCCUUUACGUCGGUGGACGU-3′

### Molecular structure prediction

Prediction of the non-complementary region of four crRNAs was performed using RNAfold (http://rna.tbi.univie.ac.at/cgi-bin/RNAWebSuite/RNAfold.cgi). The corresponding secondary structure based on the RNA sequence was obtained using RNAfold (http://rna.tbi.univie.ac.at/cgi-bin/RNAWebSuite/RNAfold.cgi), and 3DRNA (http://biophy.hust.edu.cn/new/3dRNA) was used to construct a 3D structure. At the same time, an RNA complementary sequence was constructed using BDNA (http://www.scfbio-iitd.res.in/software/drugdesign/bdna.jsp). The RNA with the most qualified conformation was chosen for visualization analysis using PyMol version 1.60.

### Docking simulations

A search was performed in the PDB database for Cas13a-nucleic acid ligand complexes (PDB: 5XWP) for crRNA and Cas13a model construction. On the basis of the template, the four crRNAs were docked to the receptor protein Cas13a to construct the 3D structure of crRNA and Cas13a. The most stable complex was chosen for visualization analysis performed using PyMol version 1.60.

### RIP

RIP was conducted using the Magna RIP kit and chromatin immunoprecipitation (ChIP)-grade anti-Cas13a FLAG antibody (DYKDDDDK Tag [D6W5B] Rabbit mAb; Cell Signaling Technology, Danvers, MA) at a dilution of 1:50 according to the manufacturer's instructions. RNA was extracted from cells as described below and transcribed into cDNA using random primers.

### RNA extraction and qRT-PCR

Total RNA was extracted from treated cells using TRIzol reagent (Invitrogen). Briefly, TRIzol reagent (0.5 mL per 1 × $10^5$–$10^7$ cells) was added directly to the culture dish to lyse the cells. Chloroform was then added at 0.2 mL per 1 mL TRIzol reagent and incubated for 2–3 min, and the lysed cell mixtures were centrifuged at 12,000 × *g* at 4°C for 15 min. The upper aqueous phase was transferred to a new tube, and 0.5 mL isopropanol per 1 mL TRIzol reagent was added, incubated for 10 min at 4°C, and centrifuged for 10 min at 12,000 × *g* at 4°C to pellet the RNA. The supernatant was removed, and the pellet was centrifuged for 5 min in 75% ethanol (1 mL 75% ethanol per milliliter TRIzol reagent) at 7,500 × *g* at 4°C, vacuum- or air-dried for 5–10 min, and dissolved in 20 μL RNase-free water. cDNAs were synthesized using the Prime Script RT Kit (Promega, Madison, WI) following the manufacturer's protocols. Quantitative real-time PCR was carried out in triplicate using LightCycler 2.0 (Bio-Rad Laboratories, Hercules, CA), and the Ct values were normalized to *GAPDH*. The final relative quantification value for target genes was expressed as $2^{-\Delta\Delta Ct}$. Experiments were repeated three times independently.

Primer pairs were as follows:

GAPDH-F: 5′-TGCACCACCAACTGCTTAGC-3′

GAPDH-R: 5′-GGCATGGACTGTGGTCATGAG-3′

Cas13a-F: 5′-TGGAAAAGTACCAGTCCGCC-3′

Cas13a-R: 5′-TCGAAGTCCTCGGTCACTCT-3′

FGFR3-TACC3-F: 5′-CCAACTGCACACACGACCT-3′

FGFR3-TACC3-R: 5′-TCCTCCTGTGTCGCCTTTAC-3′

HOTAIR-F: 5′-ATAGGCAAATGTCAGAGGGTT-3′

HOTAIR-R: 5′-TCTTAAATTGGGCTGGGTC-3′

L3MBTL1-F: 5′-AGAGGGACAACCCACTGCTA-3′

L3MBTL1-R: 5′-GGCCTTCTGCTCCTCTAGGT-3′

### Colony formation assay

U87 cells transfected with either control CON254 or FGFR-TACC3 expressing lentiviral constructs were seeded at 500 cells per well into six-well plates. After 13 days, the colonies were fixed with 4% paraformaldehyde and stained with 0.1% crystal violet. Digital images were acquired with a digital camera and colonies were counted.

### Cell viability assay

Cell proliferation was assessed using the CCK-8 assay. Cells (2 × $10^3$) were seeded into 96-well plates. At 0, 24, 48, and 72 h, medium containing 10% CCK-8 was added to cells, and plates were incubated at 37°C for 2 h. Optical density (OD) values were detected using a microplate reader (BioTek Synergy 2; BioTek, Winooski, VT).

### Cell cycle and cell apoptosis assay

Cell cycle and cell apoptosis were evaluated using flow cytometry after 48 h of exposure to the indicated treatment. The cell cycle was assessed using the Cell Cycle and Apoptosis Analysis Kit (Beyotime, Haimen, China). The apoptosis detection was performed using the Annexin V-FITC/7AAD Apoptosis Detection Kit (BestBio, Shanghai, China). After staining, the cells were analyzed using flow cytometry (BD FACSCanto II).

### Western blot assay

RIPA buffer combined with protease and phosphatase inhibitors was used to lyse the cells. Total protein lysates were extracted and centrifuged for 15 min at 4°C at 14,000 × *g*. A BCA assay kit was used to assess the protein concentrations in the supernatants. Each sample (30 μg protein) was separated using SDS-PAGE on 10% SDS acrylamide gels and transferred onto PVDF membranes. The membranes were incubated with primary antibodies against cyclin D1 (AF0931; Affinity Biosciences, Cincinnati, OH), CDK4 (DF6102; Affinity Biosciences), CDK6 (ab124821; Abcam, Cambridge, UK), caspase-3 (AF6311; Affinity Biosciences), caspase-7 (DF6441; Affinity Biosciences), and GAPDH (ab8245; Abcam) for 12 h at 4°C, followed by incubation with horseradish peroxidase (HRP)-conjugated secondary antibodies for 1 h at room temperature. The density of target protein signals was visualized using a gel imaging system (Syngene G: BOX Chemi XT4; Syngene, Cambridge, UK).

### Immunofluorescence and confocal imaging

After transduction with the lentivirus and cr1, cells were fixed with 4% paraformaldehyde and permeabilized with 0.1% Triton x-100 in PBS for 15 min. Cells were rinsed with PBS, blocked with 10% goat serum, and incubated with primary antibodies against FGFR3 at 4°C overnight (dilution 1:500; Thermo Fisher Scientific, Waltham, MA). Cells were stained with phalloidin to highlight actin (dilution 1:200; Cell Signaling Technology). Confocal images of the cells were captured using confocal microscopy (FV500) and FluoView software (Olympus, Tokyo, Japan).

### RNA-denaturing gel electrophoresis

RNA samples (10 μL) were run at 80 V for 40 min on a 1% denaturing agarose gel prepared with 1 × TAE (50 × TAE diluted in DEPC water). Electrophoresis ended when the blue dye front reached half the length of the gel, and gels were analyzed using the G:BOX F3 gel imaging system.

### Human ceRNA microarray (4*180k) analysis

Cells were divided into four groups (U87-CON254, U87-F3-T3, U87-F3-T3-Cas13a-cr1, and U87-F3-T3-AZD4547), with each group seeded in 3 wells. After treatment for 24 h, cells in the 12 wells were lysed in TRIzol. Total RNA was sequenced using the Agilent Human ceRNA Microarray 2019 (4*180k, Design ID: 086188). The threshold set for up- and downregulated genes was a fold change of $\geq 2.0$ and a p value of $\leq 0.05$. The expression of regulated genes was visualized in a heatmap. To compare the biological states or processes among four groups, GSVA was conducted using the R GSVA package (version 1.32.0). The 50 hallmark gene sets from the Molecular Signatures Database were examined to identify the pathways with noticeable changes (https://www.gsea-msigdb.org/gsea/index.jsp). Results were visualized in a heatmap.

### Gel retardation assay

pDNA (pCas13a and pCrRNA1) was diluted to 0.05 mg/mL. Polymer solutions were then added to the plasmid solutions with the same volume at various [carrier]/[pDNA] (wt/wt) ratios and vortexed. Mixtures were incubated for 10 min at room temperature, and a 20 μL volume of the complexes was analyzed with 0.6% agarose gel electrophoresis (80 V, 1 h).

### H&E and immunohistochemical staining

Sections (7 μm) were cut from paraffin-embedded tissue samples, dewaxed, and hydrated, and antigen retrieval was performed in citrate at 95°C for 30 min. Sections were incubated with primary antibody against Ki67 at 4°C for 12 h and subsequently HRP-conjugated secondary antibody for 1 h at room temperature. Visualization was performed using the substrate DAB, and sections were stained with hematoxylin and eosin. Digital images were acquired under bright-field microscopy.

### Orthotopic glioma mouse model and treatment

U87 human glioma cells ($5 \times 10^5$) were stereotactically injected into the right hemisphere of the brain in 4-week-old female BALB/c-nu mice to generate an intracranial orthotopic glioma model. Nude mice were randomly separated into four groups: U87-CON254 (control group), U87-F3-T3, U87-F3-T3-Cas13a-cr1, and U87-F3-T3-AZD4547. U87-F3-T3-Cas13a cells were transfected with 150 ng/mL crRNA1 for 24 h before implantation, and AZD4547 (50 mg/kg) was administered orally each day to the U87-F3-T3-AZD4547 group. Tumor growth was measured with bioluminescence imaging on days 7, 14, and 21. Six mice from each group were sacrificed on day 21, and brain tissues were fixed in 4% paraformaldehyde. Kaplan-Meier survival curves were generated on the basis of survival (days after implantation until death).

### *In vivo* procedure for mini-osmotic pump implantation

Seven days after intracranial tumor cell implantation, the mice were divided into four groups (n = 8 in each group) and pumps containing the following treatment solutions were secured into the backs of mice: PP/saline (vehicle control); PP/pCas13a = 1:1 (wt/wt) (denoted as both PP and pCas13a are 0.05 μg/μL, no pcr1 loaded); PP/pcr1 = 1:1 (wt/wt) (denoted as both PP and pcr1 are 0.05 μg/μL, no pCas13a loaded); and PP/pDNA = 1:1 (wt/wt) (pDNA denoted as pCas13a and pcr1 mixed at the same mass ratio). The pump systems were assembled for intracranial infusion according to the manufacturer's instructions (https://www.alzet.com/). Briefly, the agent-loaded mini-osmotic pump was placed into a subcutaneous pocket in the backs of mice. Subsequently, the osmotic pump was connected to an infusion cannula with its tip stereotactically fixed in the tumor. The pumping rate was 0.11 μL/h, and the solutions were delivered continuously for 21 days. Tumor growth was measured with bioluminescence imaging on days 7, 14, 21, and 28. Kaplan-Meier survival curves were generated on the basis of survival (28 days after pump implantation). pDNA encoding the Cas13a and cr1 were purchased from Integrated Biotech Solutions (Shanghai, China), and the polymer PP was synthesized *in vitro* by RuiXi Biological Technology (Xi'an, China).

### Statistical analysis

Statistical analysis and graphing were performed using GraphPad Prism 8 (GraphPad Software, San Diego, CA). Statistical significance was determined using an unpaired Student's t test or ANOVA for functional analysis. The correlation of samples was analyzed using two-sided Pearson correlation. The error bars in the figures are expressed as mean ± SEM. p values < 0.05 were considered to indicate statistical significance.

## SUPPLEMENTAL INFORMATION

Supplemental information can be found online at https://doi.org/10.1016/j.ymthe.2021.07.002.

## ACKNOWLEDGMENTS

This work was supported by the Tianjin Natural Science Foundation (18JCZDJC45500), the Tianjin Key R&D Plan of Tianjin Science and Technology Plan Project (20YFZCSY00360), and the Special Foundation for Taishan Scholars (tshw201502056).

## AUTHOR CONTRIBUTIONS

Kang C., Wang J., and Wu Y. designed the study. Wu Y.,Jin W., Wang Q., Zhou J., Wang Y., Tan Y., Cui X., Tong F., and Yang E. carried out the experiments. Kang C. provided technical support. Wu Y. and Jin W. performed data analysis and wrote the manuscript.

## DECLARATION OF INTERESTS

The authors have declared no competing interests.

## REFERENCES

1. Knott, G.J., and Doudna, J.A. (2018). CRISPR-Cas guides the future of genetic engineering. Science *361*, 866–869.
2. Knott, G.J., East-Seletsky, A., Cofsky, J.C., Holton, J.M., Charles, E., O'Connell, M.R., and Doudna, J.A. (2017). Guide-bound structures of an RNA-targeting A-cleaving CRISPR-Cas13a enzyme. Nat. Struct. Mol. Biol. *24*, 825–833.
3. Shmakov, S., Abudayyeh, O.O., Makarova, K.S., Wolf, Y.I., Gootenberg, J.S., Semenova, E., Minakhin, L., Joung, J., Konermann, S., Severinov, K., et al. (2015). Discovery and functional characterization of diverse class 2 CRISPR-Cas systems. Mol. Cell *60*, 385–397.
4. Granados-Riveron, J.T., and Aquino-Jarquin, G. (2018). CRISPR-Cas13 precision transcriptome engineering in cancer. Cancer Res. *78*, 4107–4113.
5. Liu, L., Li, X., Wang, J., Wang, M., Chen, P., Yin, M., Li, J., Sheng, G., and Wang, Y. (2017). Two distant catalytic sites are responsible for C2c2 RNase activities. Cell *168*, 121–134.e12.
6. Liu, L., Li, X., Ma, J., Li, Z., You, L., Wang, J., Wang, M., Zhang, X., and Wang, Y. (2017). The molecular architecture for RNA-guided RNA cleavage by Cas13a. Cell *170*, 714–726.e10.
7. Zhang, J., and You, Y. (2020). CRISPR-Cas13a system: a novel approach to precision oncology. Cancer Biol. Med. *17*, 6–8.
8. Singh, D., Chan, J.M., Zoppoli, P., Niola, F., Sullivan, R., Castano, A., Liu, E.M., Reichel, J., Porrati, P., Pellegatta, S., et al. (2012). Transforming fusions of FGFR and TACC genes in human glioblastoma. Science *337*, 1231–1235.
9. Lee, J., Lee, J., Hong, S.D., Jang, K.-T., and Lee, S.J. (2018). FGFR3-TACC3: a novel gene fusion in malignant melanoma. Precis. Future Med. *2*, 71–75.
10. Costa, R., Carneiro, B.A., Taxter, T., Tavora, F.A., Kalyan, A., Pai, S.A., Chae, Y.K., and Giles, F.J. (2016). FGFR3-TACC3 fusion in solid tumors: mini review. Oncotarget *7*, 55924–55938.
11. Lasorella, A., Sanson, M., and Iavarone, A. (2017). FGFR-TACC gene fusions in human glioma. Neuro-oncol. *19*, 475–483.
12. Di Stefano, A.L., Fucci, A., Frattini, V., Labussiere, M., Mokhtari, K., Zoppoli, P., Marie, Y., Bruno, A., Boisselier, B., Giry, M., et al. (2015). Detection, characterization, and inhibition of FGFR-TACC fusions in IDH wild-type glioma. Clin. Cancer Res. *21*, 3307–3317.
13. Jiang, T., Nam, D.H., Ram, Z., Poon, W.S., Wang, J., Boldbaatar, D., Mao, Y., Ma, W., Mao, Q., You, Y., et al.; Chinese Glioma Cooperative Group (CGCG); Society for Neuro-Oncology of China (SNO-China); Chinese Brain Cancer Association (CBCA); Chinese Glioma Genome Atlas (CGGA); Asian Glioma Genome Atlas (AGGA) network (2021). Clinical practice guidelines for the management of adult diffuse gliomas. Cancer Lett. *499*, 60–72.
14. Katoh, M. (2016). FGFR inhibitors: effects on cancer cells, tumor microenvironment and whole-body homeostasis (review). Int. J. Mol. Med. *38*, 3–15.
15. Wang, Q., Liu, X., Zhou, J., Yang, C., Wang, G., Tan, Y., Wu, Y., Zhang, S., Yi, K., and Kang, C. (2019). The CRISPR-Cas13a gene-editing system induces collateral cleavage of RNA in glioma cells. Adv. Sci. (Weinh.) *6*, 1901299.
16. Abudayyeh, O.O., Gootenberg, J.S., Essletzbichler, P., Han, S., Joung, J., Belanto, J.J., Verdine, V., Cox, D.B.T., Kellner, M.J., Regev, A., et al. (2017). RNA targeting with CRISPR-Cas13. Nature *550*, 280–284.
17. Yang, L.Z., Wang, Y., Li, S.Q., Yao, R.W., Luan, P.F., Wu, H., Carmichael, G.G., and Chen, L.L. (2019). Dynamic imaging of RNA in living cells by CRISPR-Cas13 systems. Mol. Cell *76*, 981–997.e7.
18. Butterick, T.A., Duffy, C.M., Lee, R.E., Billington, C.J., Kotz, C.M., and Nixon, J.P. (2014). Use of a caspase multiplexing assay to determine apoptosis in a hypothalamic cell model. J. Vis. Exp. (86), 51305.
19. Wang, W., Cho, H.Y., Rosenstein-Sisson, R., Marín Ramos, N.I., Price, R., Hurth, K., Schönthal, A.H., Hofman, F.M., and Chen, T.C. (2018). Intratumoral delivery of bortezomib: impact on survival in an intracranial glioma tumor model. J. Neurosurg. *128*, 695–700.
20. Tian, H., Xiong, W., Wei, J., Wang, Y., Chen, X., Jing, X., and Zhu, Q. (2007). Gene transfection of hyperbranched PEI grafted by hydrophobic amino acid segment PBLG. Biomaterials *28*, 2899–2907.
21. Gavine, P.R., Mooney, L., Kilgour, E., Thomas, A.P., Al-Kadhimi, K., Beck, S., Rooney, C., Coleman, T., Baker, D., Mellor, M.J., et al. (2012). AZD4547: an orally bioavailable, potent, and selective inhibitor of the fibroblast growth factor receptor tyrosine kinase family. Cancer Res. *72*, 2045–2056.
22. Guagnano, V., Furet, P., Spanka, C., Bordas, V., Le Douget, M., Stamm, C., et al. (2011). Discovery of 3-(2,6-dichloro-3,5-dimethoxy-phenyl)-1-{6-[4-(4-ethyl-piperazin-1-yl)-phenylamin o]-pyrimidin-4-yl}-1-methyl-urea (NVP-BGJ398), a potent and selective inhibitor of the fibroblast growth factor receptor family of receptor tyrosine kinase. J. Med. Chem. *54*, 7066–7083.
23. Kallus, S., Englinger, B., Senkiv, J., Laemmerer, A., Heffeter, P., Berger, W., Kowol, C.R., and Keppler, B.K. (2018). Nanoformulations of anticancer FGFR inhibitors with improved therapeutic index. Nanomedicine (Lond.) *14*, 2632–2643.
24. Parker Kerrigan, B.C., Ledbetter, D., Kronowitz, M., Phillips, L., Gumin, J., Hossain, A., Yang, J., Mendt, M., Singh, S., Cogdell, D., et al. (2020). RNAi technology targeting the FGFR3-TACC3 fusion breakpoint: an opportunity for precision medicine. Neurooncol. Adv. *2*, vdaa132.
25. Shi, J., Kantoff, P.W., Wooster, R., and Farokhzad, O.C. (2017). Cancer nanomedicine: progress, challenges and opportunities. Nat. Rev. Cancer *17*, 20–37.
26. Huang, D., Miller, M., Ashok, B., Jain, S., and Peppas, N.A. (2020). CRISPR/Cas systems to overcome challenges in developing the next generation of T cells for cancer therapy. Adv. Drug Deliv. Rev. *158*, 17–35.
27. Liu, Q., Zhao, K., Wang, C., Zhang, Z., Zheng, C., Zhao, Y., Zheng, Y., Liu, C., An, Y., Shi, L., et al. (2018). Multistage delivery nanoparticle facilitates efficient CRISPR/dCas9 activation and tumor growth suppression in vivo. Adv. Sci. (Weinh.) *6*, 1801423.
28. Dai, X., Park, J.J., Du, Y., Kim, H.R., Wang, G., Errami, Y., and Chen, S. (2019). One-step generation of modular CAR-T cells with AAV-Cpf1. Nat. Methods *16*, 247–254.
29. Wang, D., Zhang, F., and Gao, G. (2020). CRISPR-based therapeutic genome editing: strategies and in vivo delivery by AAV vectors. Cell *181*, 136–150.
30. Wang, D., Tai, P.W.L., and Gao, G. (2019). Adeno-associated virus vector as a platform for gene therapy delivery. Nat. Rev. Drug Discov. *18*, 358–378.
31. Zhao, X., Liu, L., Lang, J., Cheng, K., Wang, Y., Li, X., Shi, J., Wang, Y., and Nie, G. (2018). A CRISPR-Cas13a system for efficient and specific therapeutic targeting of mutant KRAS for pancreatic cancer treatment. Cancer Lett. *431*, 171–181.

**YMTHE, Volume *29***

# Supplemental Information

# Precise editing of FGFR3-TACC3 fusion genes with CRISPR-Cas13a in glioblastoma

**Ye Wu, Weili Jin, Qixue Wang, Junhu Zhou, Yunfei Wang, Yanli Tan, Xiaoteng Cui, Fei Tong, Eryan Yang, Jian Wang, and Chunsheng Kang**

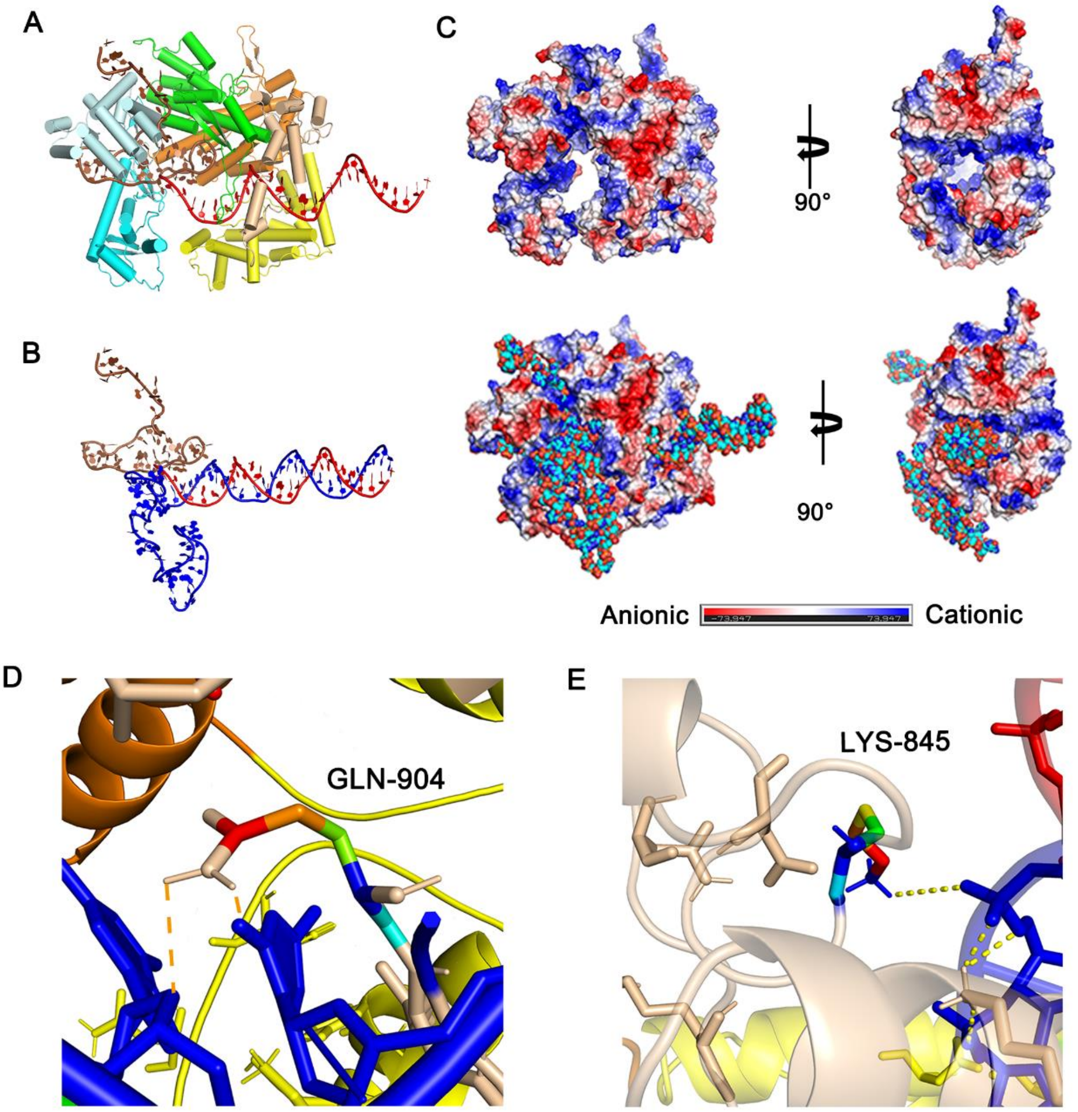

**Figure S1. Analysis of the interaction between Cas13a and RNA1.** (A) 3D structure of the Cas13a-cr1 duplex. (B) 3D structure of the crRNA1-F3-T3 duplex. F3-T3 is in blue. (C) Electrostatic binding surface analysis indicating that the negatively charged surface of RNA1 matches well with the positively charged region in the active cavity of Cas13a. (D) Partially enlarged details of the hydrogen-bond interactions of Cas13a with the bases in the 38–50-bp segment of RNA1. (E) Partially enlarged details of the hydrogen-bond interactions of Cas13a with the bases in the 51–65-bp segment of RNA1.

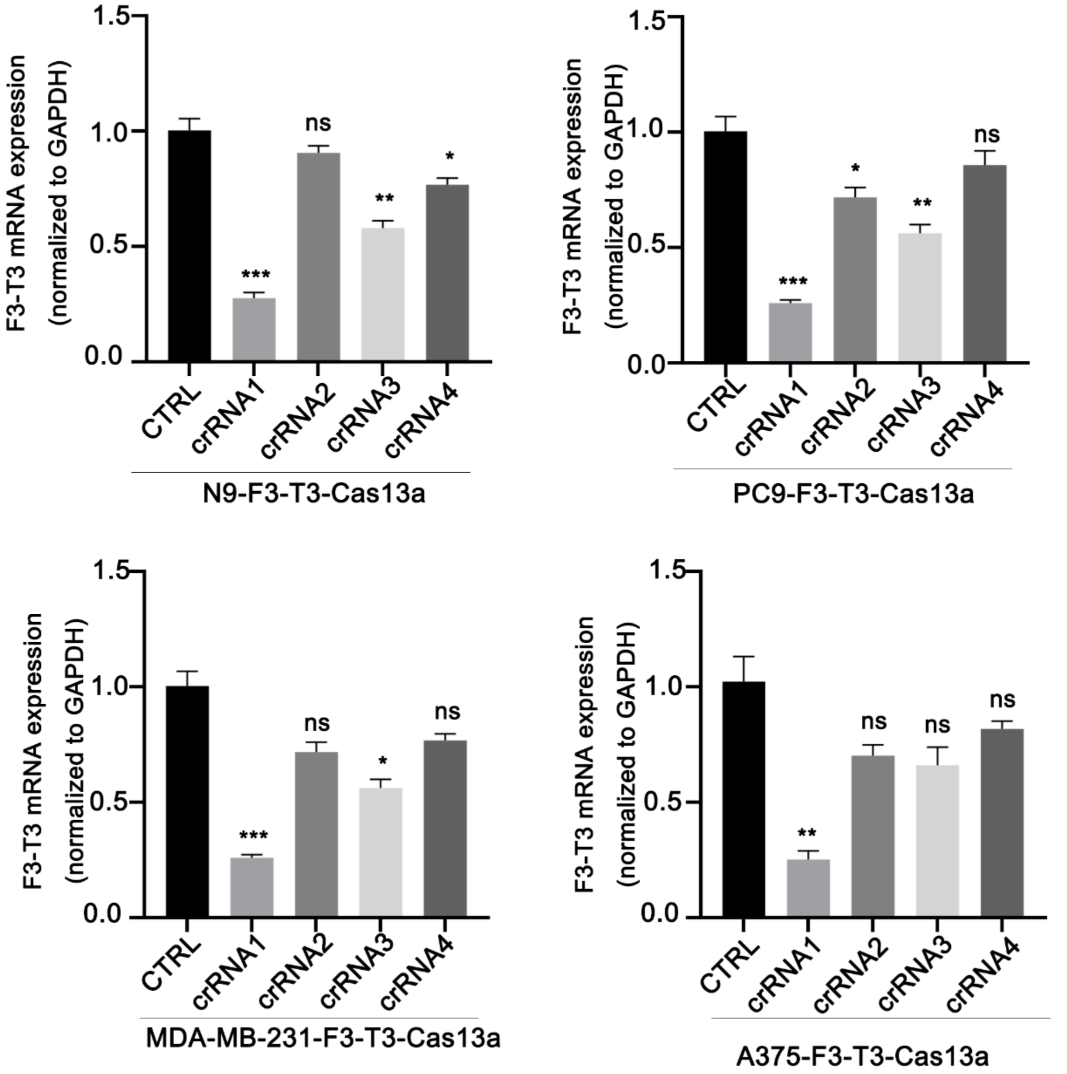

**Figure S2. Verification of Cas13a-cr1 knockdown efficiency.** Real-time PCR to assess F3-T3 mRNA levels in N9, PC9, MDA-MB-231 and A375 cells. ns represents $p > 0.05$. $^*p<0.05$, $^{**}p < 0.01$ and $^{***}p < 0.001$.

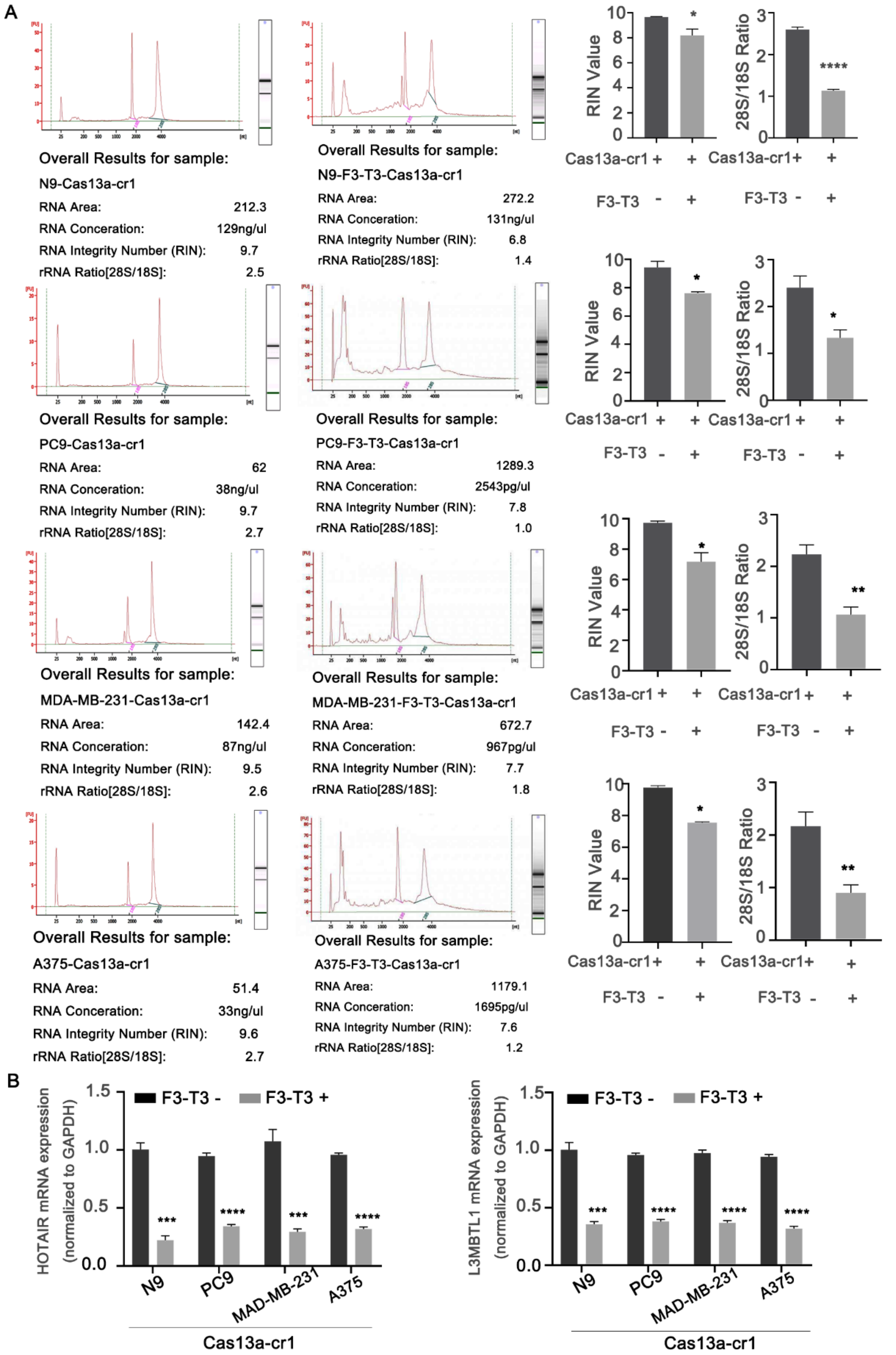

Overall Results for sample:

N9-Cas13a-cr1

RNA Area: 212.3
RNA Conceration: 129ng/ul
RNA Integrity Number (RIN): 9.7
rRNA Ratio[28S/18S]: 2.5

Overall Results for sample:

N9-F3-T3-Cas13a-cr1

RNA Area: 272.2
RNA Conceration: 131ng/ul
RNA Integrity Number (RIN): 6.8
rRNA Ratio[28S/18S]: 1.4

Overall Results for sample:

PC9-Cas13a-cr1

RNA Area: 62
RNA Conceration: 38ng/ul
RNA Integrity Number (RIN): 9.7
rRNA Ratio[28S/18S]: 2.7

Overall Results for sample:

PC9-F3-T3-Cas13a-cr1

RNA Area: 1289.3
RNA Conceration: 2543pg/ul
RNA Integrity Number (RIN): 7.8
rRNA Ratio[28S/18S]: 1.0

Overall Results for sample:

MDA-MB-231-Cas13a-cr1

RNA Area: 142.4
RNA Conceration: 87ng/ul
RNA Integrity Number (RIN): 9.5
rRNA Ratio[28S/18S]: 2.6

Overall Results for sample:

MDA-MB-231-F3-T3-Cas13a-cr1

RNA Area: 672.7
RNA Conceration: 967pg/ul
RNA Integrity Number (RIN): 7.7
rRNA Ratio[28S/18S]: 1.8

Overall Results for sample:

A375-Cas13a-cr1

RNA Area: 51.4
RNA Conceration: 33ng/ul
RNA Integrity Number (RIN): 9.6
rRNA Ratio[28S/18S]: 2.7

Overall Results for sample:

A375-F3-T3-Cas13a-cr1

RNA Area: 1179.1
RNA Conceration: 1695pg/ul
RNA Integrity Number (RIN): 7.6
rRNA Ratio[28S/18S]: 1.2

**Figure S3. Specificity of Cas13a-cr1 in various tumor cell lines.** (A) RNA integrity as assessed on the Agilent 2100 Bioanalyzer. Bars represent the mean ± SEM (n = 3). *p < 0.05, **p < 0.01 and ****p < 0.0001. (B) Real-time PCR to assess HOTAIR and L3MBTL1 mRNA levels in N9, PC9, MDA-MB-231 and A375 cells. ***p < 0.001 and ****p < 0.0001.

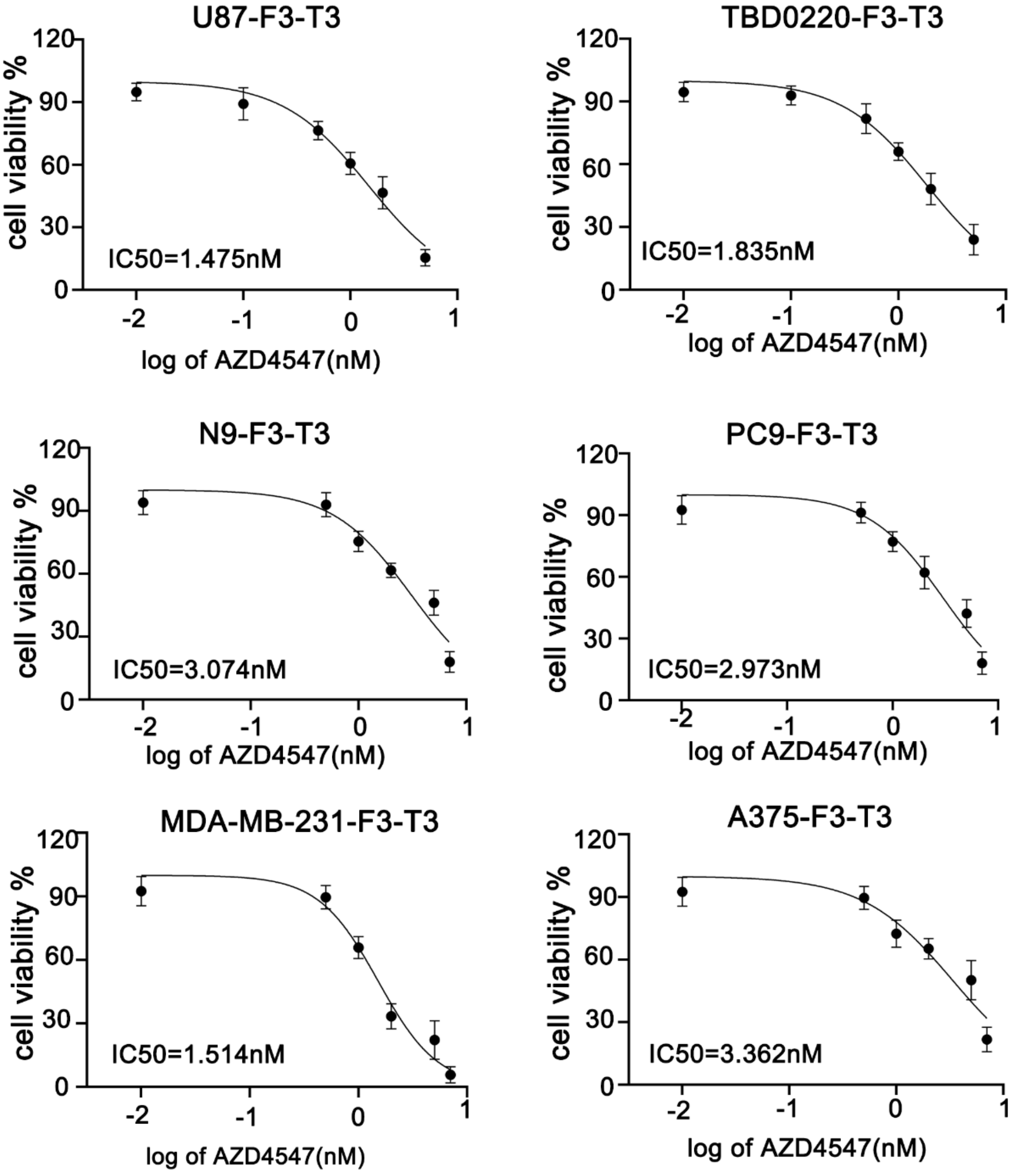

**Figure S4. IC50 of AZD4547 in different cell lines.** IC50 of AZD4547 in U87, TBD0220, N9, PC9, MDA-MB-231 and A375 cells.

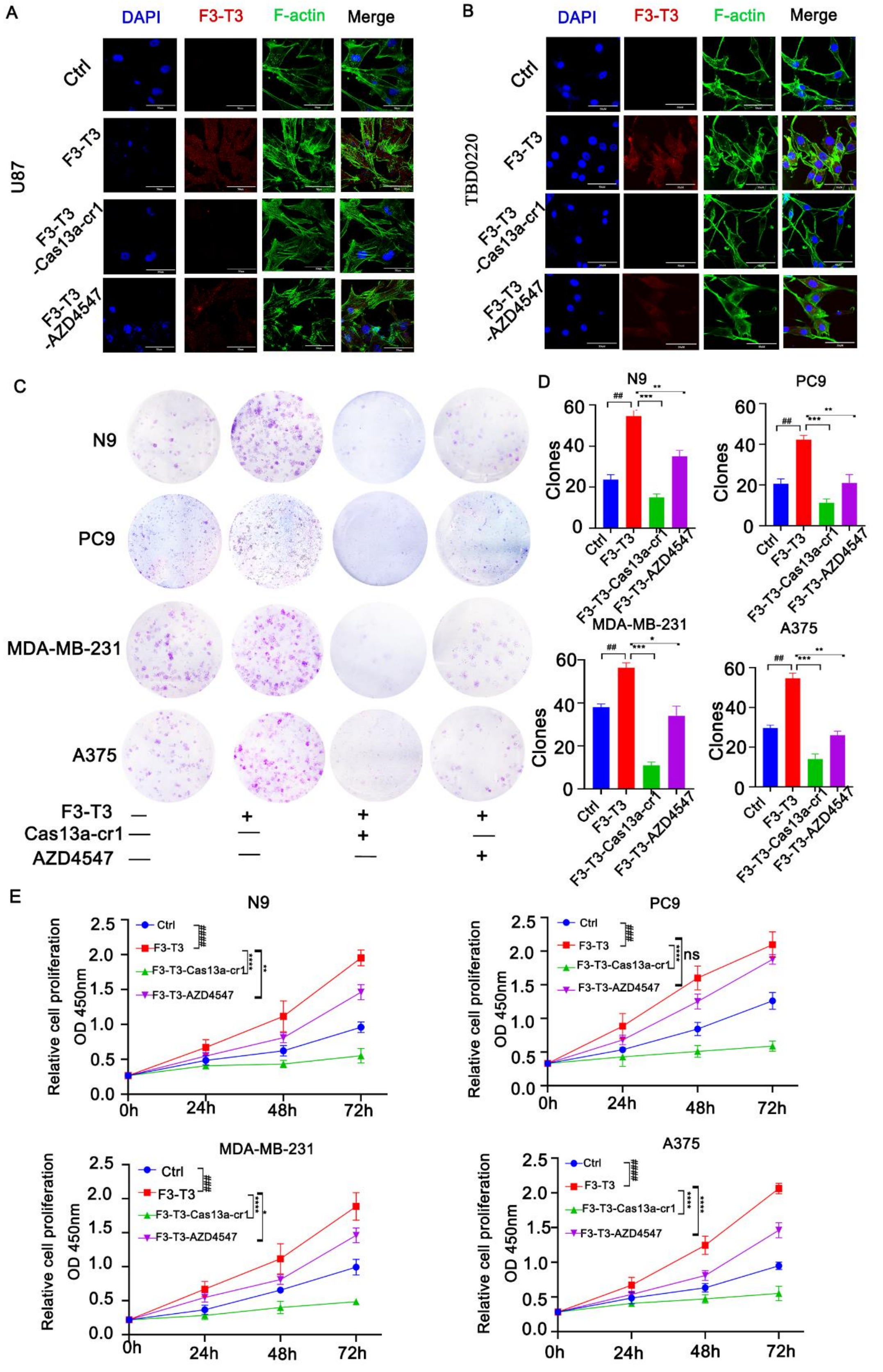

**Figure S5. Cas13a-cr1 inhibits cell proliferation in vitro.** (A and B) Immunofluorescence images captured under confocal microscopy to detect expression of the F3-T3 fusion protein. Scale bar, 50 µm. (C) Images of colony formation assays performed in N9, PC9, MDA-MB-231 and A375 cells. (D) Quantification of colony numbers in (C). ##$p < 0.01$ versus the control group. *$p < 0.05$, **$p < 0.01$ and ***$p < 0.001$ versus the F3-T3 group. (E) Growth curves generated with CCK8 assays to analyze the proliferation of N9, PC9, MDA-MB-231 and A375 cells. ns represents $p > 0.05$. ###$p < 0.001$ and ####$p < 0.0001$ versus the control group. **$p < 0.01$, ***$p < 0.001$ and ****$p < 0.0001$ versus the F3-T3 group.

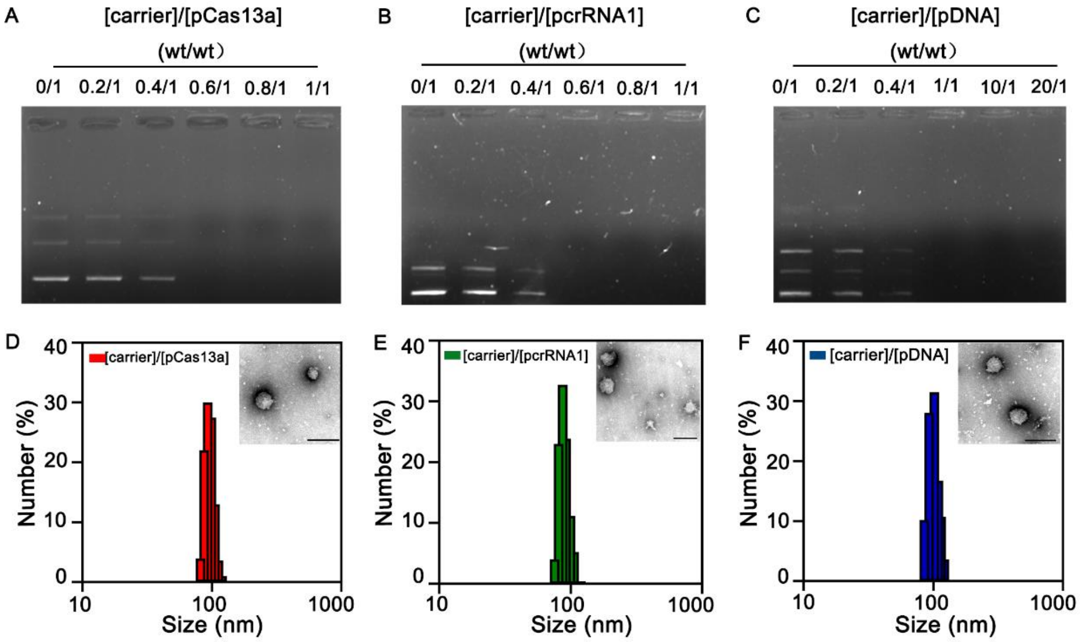

**Figure S6. Effective binding capacities of PEI–PBLG (PP) and pDNA.** (A - C) Gel retardation assay for PP. pDNA denoted as pCas13a and pcr1 mixed at the same mass ratio. (D - F) Size distribution and transmission electron microscopy images of nanoparticles. PP and plasmid DNA mixed in a 1:1 ratio (wt/wt). The scale bar is 200 nm.